Published in final edited form as:
Ann Biomed Eng. 2012 November ; 40(11): 2379–2398. doi:10.1007/s10439-012-0613-5.

Modeling to link regional myocardial work, metabolism and blood flows

James B. Bassingthwaighte[1], **Daniel A Beard**[2], **Brian E. Carlson**[2], **Ranjan K. Dash**[2], and **Kalyan Vinnakota**[2]

[1]University of Washington, Department ofBioengineering, Seattle, WA 98195

[2]Biotechnology and Bioengineering Center, Department of Physiology, Medical College of Wisconsin, Milwaukee, WI

Abstract

Given the mono-functional, highly coordinated processes of cardiac excitation and contraction, the observations that regional myocardial blood flows, rMBF, are broadly heterogeneous has provoked much attention, but a clear explanation has not emerged. In isolated and *in vivo* heart studies the total coronary flow is found to be proportional to the rate-pressure product (systolic mean blood pressure times heart rate), a measure of external cardiac work. The same relationship might be expected on a local basis: more work requires more flow. The validity of this expectation has never been demonstrated experimentally. In this article we review the concepts linking cellular excitation and contractile work to cellular energetics and ATP demand, substrate utilization, oxygen demand, vasoregulation, and local blood flow. Mathematical models of these processes are now rather well developed. We propose that the construction of an integrated model encompassing the biophysics, biochemistry and physiology of cardiomyocyte contraction, then combined with a detailed three-dimensional structuring of the fiber bundle and sheet arrangements of the heart as a whole will frame an hypothesis that can be quantitatively evaluated to settle the prime issue: Does local work drive local flow in a predictable fashion that explains the heterogeneity? While in one sense one can feel content that *work drives flow* is irrefutable, there are no cardiac contractile models that demonstrate the required heterogeneity in local strain-stress-work; quite the contrary, cardiac contraction models have tended toward trying to show that work should be uniform. The object of this review is to argue that uniformity of work does not occur, and is impossible in any case, and that further experimentation and analysis are necessary to test the hypothesis.

Keywords

Excitation-contraction coupling; coronary blood flow; cellular metabolism; phosphorylation potential; oxygenation; blood-tissue exchange processes

Introduction

From the times of the early observations using microparticle deposition to estimate regional myocardial blood flow distributions [104,14,134,86] (Richmond 1970; Bassingthwaighte 1972; Yipintsoi, 1973b; Marcus 1977), people were curious about the reason for the heterogeneity. The first thought was that the heterogeneity was random variation in the methods due to

Address for Correspondence: James B. Bassingthwaighte, M.D., Ph.D., Department of Bioengineering, University of Washington, Box 35-5061, 1705 NE Pacific St., Seattle, WA 98195-5061, Phone: (206) 685-2012 and FAX (206) 685-3300.

Bassingthwaighte JB, Beard DA, Carlson BE, Dash RK, and Vinnakota K. Modeling to link regional myocardial work, metabolism and blood flows. Ann Biomed Eng 40(11): 2379-2398, 2012.

particle heterogeneity, variability at branch points, and temporal variation. A next thought was that it was due to variations in flows in the branching networks of the coronary arteriolar system. Later, when it had been worked out that the heterogeneity due to the methods amounted to only a few percent of the observed of regional flows, it was thought to be temporal variation, fluctuations in the resistance in smaller arteries and arterioles, as had been seen in skeletal muscle. But King et al[74] [1985] observed the flow distributions in awake baboons with high resolution and found the same degree of heterogeneity seen earlier with the cruder methods, and further, found that the flows in individual regions were actually rather stable relative to the mean flow for the heart [75](King 1989).

Deeper analyses revealed that near neighbor regions tended to have similar flows. The near-neighbor spatial correlation was self-similar, that is, the decrement in correlation diminished proportional to distance in logarithmic fashion. This led to a series of studies documenting the fractal nature of the spatial heterogeneity [119](van Beek 1989), and stimulated analyses of the washout characteristics, which for flow-limited solutes like ^{15}O-water [28](Beard 2000a) and antipyrine [132](Yipintsoi 1970) turned out also to have fractal, power law, time courses. The washout could be “explained” by models of the branching of the coronary network [119,29](van Beek89; Beard2000b), and have been observed in the modeling of flows through vascular networks reconstructed from the anatomic data on the vessels [29,70](Beard 2000b; Kassab93). This raises the question of why the networks had this particular kind of heterogeneity, and whether or not the network was simply adapted to the need to deliver nutrients locally.

It was long known that oxygen consumption and coronary blood flow were increased in proportion to increases in the work of the heart. Such observations don’t distinguish a homogeneous myocardium from a heterogeneous one, but are most easily explained if all regions, homogeneous or heterogeneous, changed flow proportionately.

“Experiments of nature”, most particularly myocardial infarction and left bundle branch block, led to cardiac remodeling, for example, ventricular wall thickening and increasing blood flow in regions called upon to increase their work load in response to the disorder. In LBBB the septal region is activated early compared to the rest of the left ventricle (LV) [101](Prinzen 1990). It also changed metabolic profile, diminishing glucose uptake, even to the extent of raising suspicions that the septum was ischemic [5](Altehoefer98), though it turned out later that while glucose uptake was down, flow per gram of tissue was near normal. But in the late-activated LV regions that were doing *more* work, the glucose uptake increased; the LV free wall thickened, hypertrophied. Starling [96][Patterson14] had shown that prestretch of the myocardium by extra filling at the end of diastole evoked a stronger contraction on the next beat. Does this imply that the pre-activation lengthening can lead to remodeling? The left ventricular free wall hypertrophy in LBBB and the hypertrophy of the undamaged myocardium around the edges of an aneurysmal infarcted region are certainly in accord with this possible causation.

The suggestion is therefore that *regional* cardiac force development and work drives *regional* responses in metabolism, energy production, *and initiates the adaptation to load*, the process of remodeling and localized hypertrophy. We review here the cause and effect relationships, and extend the perspective to identifying potential experiments that are needed to test the validity of our current assumptions and concepts.

SECTION I. The broad heterogeneity of regional myocardial blood flows, rMBF

The first observations of the heterogeneity of rMBF were made using gamma camera imaging of deposits of macroaggregated albumin injected into the aorta in isolated blood perfused dog hearts [104](Richmond70). The interpretation was that the heterogeneity was artifactual, the error being caused by the particles being of widely varied sizes. When polystyrene microspheres were first used the same issue of nonuniformity of size was considered to be the prime source of the variation, though it was clear that a big contributor to the variation was in the statistics of the small numbers of microspheres per unit mass of tissue [134](Yipintsoi 1973b). One source of bias was that the larger spheres, over 25μm in diameter, tended to flow in the central streamlines of the penetrating arterioles running perpendicularly through the wall, and so overestimated sub-endocardial flows. When the technology advanced to produce spheres of virtually uniform sizes, comparisons of the depositions of spheres of different sizes led to a standard procedures of using 15 μm spheres: ones of 10 μm were less than 100% trapped, ones of 25 to 50μm appeared biased and those of 12 to 16 μm were trapped and appeared unbiased, though this was not proven until the “molecular microsphere” technique evolved[83](Little83). The evidence [18](Bassingthwaighte 87 spheres) was that microsphere estimates of regional flows were reliable. The data on the heart of dogs, pigs, sheep, baboons, rabbits, guinea pigs, and hamsters all showed that the heterogeneity was about 25 to 30% at a spatial resolution of about 1% of the heart size; this was consistent, independent of cardiac size or species. (Comment: fluorescent microspheres are more reliable than radioactive spheres for studies extending over months because the fluorescent dyes leach out of the spheres more slowly than do the radioactive labels [102] [Prinzen 2000].)

What was particularly interesting was that the pattern of relative flows in individual hearts was stable over time; repeated microsphere injections gave remarkably similar results each time. A particular study on awake baboons [74](King et al 1985) with sequences of 6 repeated microsphere injections during periods of rest, exercise or mild heat stress showed that the regional flows maintained the same distribution, relative to the mean flow, through all of these states. As shown in Figure 1, the density function of regional myocardial blood flows, rMBF, in the left ventricle (dotted line) ranged from about 30% of the mean flow to over twice the mean flow, almost a ten-fold range of flows. In comparison of the flow in any specific region to later or earlier measures within a 24 hour period, a regional flow that was 50% of the mean flow or less was never found later to be as high as the mean flow on 5 subsequent observations. Nor did a region with local flow of 150% of the mean or greater ever decrease to the mean flow on the 5 subsequent observations. This remarkable stability held even through three to four-fold changes in the mean myocardial blood flow [75](King and Bassingthwaighte 1989).

To determine microsphere measurement error, we developed a “molecular microsphere”[18], a molecular marker that was nearly 100% taken up by the heart tissue during single passage: small molecules cannot be biased by fluidic forces at branch points as can hard spheres of nearly arteriolar dimensions, and therefore their deposition regionally should be purely proportional to the flow. The “molecular microsphere” iodo-desmethylimipramine (IDMI), which binds firmly to serotonin receptor sites, and standard 15 μm spheres, were injected simultaneously into the left atrial cavity of dogs so the spheres were well mixed in the blood before entering the coronaries. Using two different IDMI labels and 4 different microsphere labels, the standard deviation of estimated flow for a 200 mg region was about 2% for IDMI and 7% for 15 μm spheres, much less than the variation within each left ventricle, 25 to 30%, at the same piece size resolution. This gave a clear evaluation of the situation; variation due to measurement error is far too low to explain the heterogeneity in rMBF.

Shortly thereafter we found that we could replace radioactive tracers by using the microspheres labeled with fluorescent markers. The estimates did not differ, and fluorescent spheres have been in common use since [55,121,102](Glenny 1993; van Oosterhout 1998; Prinzen 2000). Having learned that the heterogeneity of regional myocardial blood flow was large, and stable, it made sense to try to figure out the nature of that heterogeneity, as a step toward finding its cause.

SECTION II. The fractal nature of regional myocardial blood flows, rMBF

A clue was that the variation was not due to random fluctuations over time, for the flow in individual regions was relatively constant when conditions were not changing, and when there were large changes in cardiac work and coronary blood flow, the tendency was for the flows to change roughly proportionately everywhere.

Heterogeneity is described quantitatively by calculating the variance of the distribution; equally good in reporting is the standard deviation or the relative dispersion, RD. The RD is the standard deviation divided by the mean, and known in statistics as the coefficient of variation. The measurement of variance of something over a spatial domain is problematic in that the choice of unit size is arbitrary. The fundamental problem is that the more refined the spatial resolution used, the greater is the *apparent* variance, as in Fig. 2. This is true for population densities (by country, province, county, township, square kilometer) and for tissue properties [17](Bassingthwaighte, Liebovitch, and West 1994). For regional flows in the heart the variations are not random: there is correlation in flows among near-neighbor regions as one might expect from the nature of a dichotomously branching system [133,23](Yipintsoi 1973a; Bassingthwaighte, Yipintsoi, Harvey 1974). The correlation can be found either by the method of fractal dispersional analysis described by Bassingthwaighte, King and Roger [16][1989] and by van Beek [119][1989] or by looking at the spatial autocorrelation structure [12](Bassingthwaighte and Beyer, 1991). The nearest-neighbor correlation coefficient, r_1, is related to the fractal dimension D, $r_1 = 2^{3-2D} - 1$. The spatial autocorrelation function between neighbors separated by $n - 1$ pieces of a given size, r_1, r_2, … r_n, falls off as a power law function of the distance. This power law scaling in the autocorrelation and between the log apparent heterogeneity and the log of the spatial resolution is a fractal, demonstrating the self-similarity. The self-similarity, or correlation fall-off, is independent of actual location. The diminution in apparent heterogeneity with larger tissue samples is the same for any specific percent enlargement, independent of the actual unit size.

The fractal dimension, D, is 1.20 to 1.28 for regional myocardial flow distributions, rMBF; the near-neighbor correlation coefficient, r_1, is about 0.6. The Hurst coefficient, [67](Hurst 1951) H equals $2 - D$. It is named after the British engineer and hydrologist who first analyzed the correlation structure in the Nile River flows recorded over a millennium [114](Sutcliffe, 1979). He calculated it as the range of cumulative deviations from the mean divided by the standard deviation; later this was found to give biased estimates, and improved methods are now used [38](Cannon 1997). High values of H, $0.5 < H < 1$, indicate smoothness and a high r_1, that is a high degree of contiguity in successive years, the years of famines and then of floods. Low H, $0 < H < 0.5$, indicates roughness and negative r_1, with a high tendency to alternate levels below and above the mean. With $H = 0.5$ the relationship is purely random, with zero correlation. The description of the diminution in correlation with distance, or the number of intervening units or tissue volume elements, is given by the expression for correlation between the nth units [85] [Mandelbrot and van Ness]:

$$r_1 = \frac{1}{2}\{|n+1|^{2H} - 2|n|^{2H} + |n-1|^{2H}\}, \quad (1)$$

where n is the number of units of any chosen uniform size.

This expression fits cardiac data at two different volume element sizes (Fig. 3). The analysis is a self-similarity test: it tests whether or not the same relationship for the correlation falloff holds for two different piece sizes. It does, thus fulfilling the standard fractal phrasing "self-similarity independent of scale". The autocorrelation function for n > 2 is a power law function:

$$r_n/r_{n-1}=[n/(n-1)]^{2H-2}. \quad (2)$$

The line shown in Figure 3, when plotted on log-log axis, becomes straight for n > 2. That these regional flows are fractal is not an explanation, but is an important statistical description of the heterogeneity *and* the correlation, and provides a basis for relating structure to function. A recommendation on how the observed heterogeneity should be reported can be derived by taking a utilitarian view about the spatial resolution: from a point of view of refined measures of regional flows, resolution better than 500 tissue pieces of a heart of 200 g is seldom exceeded; this is 0.2% of total mass. When a heart is cut into 500 pieces the RD can always be calculated for larger pieces by combining *nearest-neighbor* regions and redoing the calculation. The RD *must* decrease monotonically with increasing tissue unit size, as in Fig. 2; the aggregation process neglects the variations between subunits since each is regarded as if it were internally uniform. For standardizing the reporting of heterogeneity one could choose a particular unit size, e.g. 1 gram and give the value of D or H. To compare mouse and human hearts, a better standardization is to report RD at a particular *fractional* mass, e.g., at 1% of the LV mass as in Fig. 2. An alternative is to report both the RD and the fractal dimension as in the expression:

$$RD(m)=RD(m_0) * (m/m_0)^{2-D} \quad (3)$$

where m is the particular tissue unit size, grams, m_0 is an arbitrary reference size, e.g., 1 gram, and D is the fractal dimension, giving $RD(m) = 0.232\ m^{-0.178}$; the value 0.232 is m_0 the $RD(m = 1\ g)$. Choosing m_0 as 1% of LV mass would give generality in the reporting since $RD(m_0)$ would give the reference value directly. For the data from the 50g heart in Figure 2 with 1% of mass being 0.5 g, the $RD(m = 0.5\ g) = 0.262$.

The spatial correlation is self-similar, as is illustrated in Figure 3. The correlation falloff as a function of distance is the same at two different levels of aggregation. The aggregation lumps nearest neighbors together, a process that is repeated to produce the RD plots like Figure 2. The nearest neighbors in the heart are in 3-space so each piece can pair with any of several nearest neighbors to form an aggregate of twice the size. In Figure 3 the correlation falloff is shown for two sizes. The same fractal dimension, D = 1.27, fits both relationships, demonstrating the self-similarity.

The next question is "What gives rise to the fractal characteristics of the flow distributions?"[72][Kendal 2001]. A probable cause is the nature of the vascular branching; van Beek[20,119] (Bassingthwaighte and vanBeek 1988, 1989) found that a dichotomous branching system with a small degree of asymmetry in flows in successive branches sufficed to give the observed flow heterogeneities and fractal dimensions. Data on many vascular trees of a variety of organs have been observed to be self-similar, as illustrated in Figure 4 by constancy of the ratios of the lengths of parent to daughter segments of the left anterior descending coronary artery of pigs by Kassab et al [70][Kassab1993]. Log-log relationships are also found for diameters. One can expect there to be correlation in flows amongst vessels having common feeder vessels and identical pressure heads. The high degree of correlation

r_1 between nearest neighbor regions seems to affirm this because it is most likely that neighboring regions are supplied by common parent vessels.

But blood vessels grow in response to local needs. Taking this view, it may be better to think of the tissue requirements as the stimulus for vessel growth. A variety of models can be shown to fulfill growth processes ending up with fractal flow distributions. A three-dimensional space filling model [28] [Beard and Bassingthwaighte, 2000a] was based simply on sending out successive branches using exactly the statistics of Kassab's data[70] [Kassab 1993] but positioning them for maximal avoidance of previously positioned branches. The result was a network that provided flow distributions with the same fractal dimension as the animal hearts, the same correlation structure, the same density of blood vessels and the same levels of flow. Furthermore the washout characteristics of the network followed the same power law relationship, log tissue residue versus log time, as was found for ^{15}O-water washout from isolated dog hearts [11][Bassingthwaighte and Beard 1995] Now given that there was no overt growth stimulus from the empty shell into which the vessels grew, one could believe that the vessel growth sufficed as an explanation. The counterargument is of course that the avoidance of established vessels forced the new vessels to be placed in regions devoid of vessels, exactly the same regions that might be hypoxic and sending signals promoting growth. Thus, even if lacking proof, it is logical to expect the requirements for nutrients to find its basis in regional contractile stress, strain and coordinated contraction.

Pries and Secomb [100][2009] constructed microvascular networks based on the anatomy of thin tissues with low metabolic rates and, from observing that structural adaptation including response to local needs only partially compensated for this heterogeneity, they derived the view that a residual degree of heterogeneity was due to the network structure which could not be further adapted. This may apply to mesentery and cremaster, or even brain [108](Secomb 2000), but the cardiac adaptations to prolonged dyssynchrony appear relatively complete [122](van Oosterhout 2002) and would argue against extrapolating their ideas to the heart. In contrast, acute changes such as catecholamine infusion (increasing contractility and work), and hypoxia or adenosine infusion (causing coronary vasodilation) result in rapid redistribution of flows within a minute or two [135](Yipintsoi 2012)

SECTION III

Oxygen Delivery and Exchange: From Hemoglobin to Cellular Metabolism

Oxidative energy metabolism in muscle cells, including mitochondrial ATP synthesis from carbohydrate and fatty acid substrates, is intimately coupled to the blood flow and O_2 delivery by the microcirculation [34][Beard 08]. ATP is required to maintain the contractile function of the muscle and many other key cellular processes [9][Bassingthwaighte 2001]. Since O_2 is highly extracted from the blood and is rapidly consumed in the cells of many tissues, O_2 tension (P_{O2}) varies spatially in the microvasculature, from about 100 mmHg near the inflow into capillaries to as low as 20–40 mmHg near the outflow in metabolically active organs such as the heart [30](Beard 2001a). Therefore, the transport of O_2 and other key solutes to tissue is an inherently a spatially distributed process requiring partial differential equations. Mathematical modeling and computer simulations of blood-tissue O_2 and solute exchange are used in analyzing experimental data on cell and tissue/organ function and testing hypotheses during changing physiological conditions such as ischemia (low blood flow), hypoxia (low O_2 supply), and exercise (high energy demand)[33,26,44,128] [Beard03;Beard06;Dash06;Wu07]. Such simulations are also helpful in interpreting experimental data from tracer studies involving tracer-labeled ^{15}O and ^{17}O-oxygen and other substrates. Modeling the transport of tracer ^{15}O oxygen and its metabolic byproduct tracer ^{15}O water is key to interpreting the results from positron emission tomographic (PET)

imaging to estimate local perfusion and metabolism in the heart [46,82][Deussen96; Li 97]. Similarly, understanding the effects of changing blood flow on local blood and tissue O_2 concentration is important in interpreting the physiological significance of blood-oxygen-level-dependent (BOLD) contrast magnetic resonance imaging (CMRI) [73,94][Kettunen2002; Ogawa93] and ^{17}O nuclear magnetic resonance imaging (NMRI) [97.98](Pekar91; Pekar 1995] in the working brain.

Oxygen Transport to Tissue

The process of O_2 transport and metabolism in the microcirculation involves convection, diffusion and hemoglobin-facilitated transport in the blood, permeation across the capillary and cell membranes, diffusion and myoglobin-facilitated transport in the tissue, and finally consumption by many interacting biochemical reactions inside the mitochondria of the muscle cells [11,99,61][Bassingthwaighte 84; Popel89; Hellums96]. Many mathematical models have been developed for understanding various aspects of this complex problem and for interpreting experimental data and testing physiological hypotheses behind the experiments[15]. The classical Krogh tissue cylinder model [79] [Krogh, 1919], a single cylindrical tissue unit supplied by a single capillary, has been the basis of most of the theoretical studies on O_2 transport to the tissue over the past decades [99,61,53,58,59][Popel89; Hellums96; Federspiel 86; Groebe90; Groebe and Thews 90] for steady-state analyses and [46,82,35][Deussen96; Li97; Beyer2002] for tracer transient analyses. Simplified compartmental models have also been developed and used in dynamic PET imaging [66,88][Huang 86; Mintun84] and BOLD CMRI [73,94][Kettunen02; Ogawa93] studies of cerebral O_2 utilization. Other models based on non-Krogh geometry have been designed/proposed to reflect the anatomical and morphological structures of the specific vessels and tissues [33,24,29,28,30][Beard03; Beard01b; Beard00b; Beard and B00b; Beard and B01a]. These models are based on the assumption of constant P_{CO2}, pH, 2,3-diphosphoglycerate (DPG) concentration and temperature in the microcirculation. However, all these variables affect the dynamic transport and metabolism of O_2 in the microcirculation (see below). A descriptive model of the system must consider integration of the anatomical and morphological structures of the specific vessels and tissues along with the physical, physiological, and biochemical processes that govern the transport and metabolism of O_2 in the microcirculation.

Factors Affecting Oxygen Transport to Tissue

The delivery of O_2 to tissue is characterized by a complex system of physiochemical processes, as schematized in Figure 5. It depends on simultaneous release of CO_2 from the tissue (a waste-product of oxidative energy metabolism) as well as on bicarbonate (HCO_3^-) buffering, acid-base balancing, and hemoglobin-mediated nonlinear O_2-CO_2 interactions inside the red blood cells (RBCs) [54][Geers 00]. For example, a decrease in pH or an increase in P_{CO2} in the systemic capillaries decreases the O_2 saturation of Hb ($SHbO_2$) and increases the O_2 delivery to the tissue (the Bohr effect: shifting the oxygen saturation curve to higher PO_2s). On the other hand, an increase in P_{O2} in the pulmonary capillaries decreases $SHbCO_2$, the CO_2 saturation of Hb (the Haldane effect), and so in the lung increases the rate of CO_2 removal from the blood to alveoli. Consideration of both the Bohr and Haldane effects is important in establishing the Hb-mediated nonlinear O_2-CO_2 interactions. Raising the temperature, as in working muscle, also decreases the O_2 binding to Hb and so further facilitates O_2 delivery from blood to tissue.

In view of these complex phenomena, the interpretation and understanding of the alveoli-blood or blood-tissue gas exchange, whether being assessed from the observations of arterial and venous O_2 concentrations, or by intra-tissue chemical signals such as BOLD Contrast MRI or NMRI, or by external detection of tracer contents such as ^{15}O-oxygen and ^{15}O-

water through PET imaging, depends in general on all the factors involved in the dissociation of HbO_2 and $HbCO_2$. Thus, the modeling of O_2 transport and metabolism must account for the coupled transport and exchange of CO_2, HCO_3^- and H^+ as well as nonlinear O_2-CO_2 interactions inside the RBCs due to the competitive binding of O_2 and CO_2 with Hb.

In order to quantify the Hb-mediated nonlinear O_2-CO_2 interactions and the Bohr and Haldane effects, Dash and Bassingthwaighte [43,44,45][Dash06;Dash04;Dash10], have developed new mathematical models for the O_2 and CO_2 saturations of Hb (S_{HbO2} and S_{HbCO2}) from the equilibrium binding of O_2 and CO_2 to Hb inside the RBCs. They are in the form of *invertible* Hill-type equations (as used for Figure 6) with the apparent Hill constants K_{HbO2} and K_{HbCO2} dependent on P_{O2}, P_{CO2}, pH, [2,3-DPG], and temperature in the blood. The invertibility of these equations enables analytical calculations of P_{O2} and P_{CO2} from S_{HbO2} and S_{HbCO2} and vice-versa. (This is not to be confused with the *reversible* Hill equation put forward by Hofmeyr and Cornish-Bowden [64](1997) for cooperative enzymes.) This is especially important in the computational modeling of simultaneous (dynamic) transport and exchange of O_2 and CO_2 in the alveoli-blood and blood-tissue exchange systems, allowing one to account efficiently for the rapidly changing conditions along the length of the capillary (in lung or metabolizing tissue). The HbO_2 and $HbCO_2$ equilibrium dissociation curves computed from these models are in good agreement with the previously published experimental and theoretical curves in the literature [36,126,71,110][Buerk 86; Winslow83; Kelman 66; Severinghaus 79].

Simultaneous Oxygen and Carbon Dioxide Transport and Exchange

There have not been many studies in the literature on simultaneous transport and exchange of O_2 and CO_2 in the microcirculation that account for spatial gradients of O_2 and CO_2. Hill et al.[62,63][Hill73a,73b] and Salathe et al. [106][1981] have studied the kinetics of O_2 and CO_2 exchange through compartmental modeling by accounting for the physiochemical processes discussed above, including the acid-base regulation, but not network geometry. However, Goldman and Popel [56] did in addition account for convection and diffusion in complex networks (including concentration gradients along the capillary length), an important feature of O_2 and CO_2 transport and exchange in metabolically active tissues like the myocardium. Huang and Hellums [65][Huang 94] developed a computational model for the convective and diffusive transport and exchange of O_2 and CO_2 and acid-base regulation in the blood flowing in microvessels and in oxygenators by accounting for the Bohr and Haldane effects, the nonlinear O_2-CO_2 interactions quantitated by Dash[45] (2010) shown in Figure 6. The review by Hellums et al.[61] [Hellums96] captures these phenomena well, even though they do not account for production of CO_2 in muscle and its further facilitation of O_2 release from Hb.

Dash and Bassingthwaighte [44][2006] included metabolic O_2 consumption and CO_2 production in modeling the simultaneous transport and exchange O_2 and CO_2 for analyzing experimental data related to muscle cellular energetics. Since the pH variations in blood and tissue influence the transport and exchange of O_2 and CO_2 (via the Bohr and Haldane effects), and since most of the CO_2 is transported as HCO_3^- via the CO_2 hydration (buffering) reaction, the transport and exchange of H^+ and HCO_3^- were also simulated along with that of O_2 and CO_2. This model, using invertible Hill equations for the O_2 and CO_2 saturations of Hb (S_{HbO2} and S_{HbCO2}) allows efficient calculation of P_{O2} and P_{CO2} from S_{HbO2} and S_{HbCO2} along the length of the capillary during dynamic simulation of the model under dynamically changing conditions (ischemia, hypoxia and exercise).

Analysis of Tracer ^{15}O-oxygen and ^{15}O-water in PET imaging

The positron emission tomography (PET) imaging technology using radiolabeled ^{15}O-oxygen and ^{15}O-water has largely been developed for discovering information related to local perfusion and metabolism in the myocardium and brain. Modeling the transport of tracer ^{15}O-oxygen and ^{15}O-water in blood-tissue exchange systems is therefore important in interpreting the residue and outflow dilution curves from dynamic PET imaging. To model these high temporal resolution tracer transient data, one needs a physiologically realistic and computationally efficient model.

Compartmental, stirred tank models assume uniform concentrations along the length of a capillary-tissue exchange region and cannot fit high temporal resolution data. Therefore axially-distributed models [8,13,15,22,][Bassingthwaighte et al 74; 89; 92] as in Figure 7 were developed to handle solute exchanges in a general way. Li et al.'s [82][Li97] nonlinear model is computationally efficient and has been used in the analysis of ^{15}O-oxygen and ^{15}O-water tracer transient data [time activity curves (TAC) obtained through the region of interest (ROI) analysis] in dynamic PET imaging to estimate the regional myocardial blood flow (MBF) and regional metabolic rate of oxygen (MRO_2). While it has long been generally accepted since the work of Starling [96](Patterson 1914) and Evans and Matsuoka [50](1915) myocardial oxygen consumption is proportional to overall cardiac work, it is not yet demonstrated that this holds at the regional level. Figure 8 shows that MBF and MRO_2 correlate linearly under varying physiological conditions. The model of Li et al. [82](1997) was based on the assumptions of (1) equilibrium binding of oxygen with hemoglobin and myoglobin, and (2) constant levels of P_{CO2}, pH, 2,3-DPG and temperature. Dash [44][Dash06] augmented the linear models to take into account for the dynamic system behavior under varying physiological conditions, including the detailed kinetics of oxygen binding to hemoglobin and myoglobin, and the effects of P_{CO2}, pH, 2,3-DPG and temperature on the binding [45][Dash 2010]. An additional factor comes into play when high specific activity ^{15}O-oxygen coming straight from the cyclotron is injected or inhaled: the ^{15}O-oxygen concentration is not at tracer levels but is so high that it competes with the ^{16}O-oxygen for the binding sites on Hb. The solution to this is to use a dual model, accounting for both ^{16}O-oxygen and ^{15}O-oxygen and their competition for the Hb binding sites. A breath of ^{15}O-oxygen at high pO_2 displaces the ^{16}O-oxygen from hemoglobin.

Blood flow through the microvasculature is intimately controlled to match the dynamics of O_2 release from Hb, diffusion into the surrounding tissue, and consumption in the tissue cells. The specific details on how this regulation is influenced by vascular and cellular level dynamics are still the subject of much conjecture. The vascular regulatory response to local stimuli such as pressure and flow has been well documented, but how cellular metabolism affects the control of vascular blood flow is less well understood. In myocardial tissue, studies of coupled O_2 transport and energy metabolism have been made, however a detailed quantitative analysis of the complex dynamics including interactions between the release of O_2 from RBCs, utilization of O_2 in the cell and the response of the vascular system to O_2 demand has not been explored. A major reason is the difficulty in obtaining the detailed information needed to integrate realisitically all the model components.

SECTION IV. Modeling and Analysis of Cardiac Metabolism

The next phase is to develop computational models to describe regulation of blood flow and the transport of O_2 and other key substrates (e.g., glucose, lactate, fatty acids) from the microvasculature into the surrounding tissue of the myocardium as demanded by the underlying cellular and subcellular metabolic mechanisms. Such models will account for the axially-distributed (radially-lumped) advection and diffusion of species in the blood along with diffusion and reaction of the species in the tissue. They must incorporate the

mechanisms of cooperative binding of O_2 with hemoglobin (Hb), non-cooperative binding of CO_2 with Hb, and nonlinear O_2-CO_2 counterinfluences as well as bicarbonate buffering, and pH. In cytosol and mitochondria they must account for the linked metabolic pathways for ATP hydrolysis, creatine kinase, adenylate kinase, glycolysis, fatty acid metabolism, tricarboxylic acid (TCA) cycle, and oxidative phosphorylation. Regulation at the vascular level will include local responses to pressure and shear stress in the vessel in addition to ATP and NO release from the RBCs which can trigger an upstream conducted dilatory response. These models will further advance our understanding of the influence of mitochondrial metabolic mechanisms on microvascular blood flow and O_2 transport and will have future applications for the description of flow heterogeneities in cardiac tissue exhibiting physiological and pathophysiological mitochondrial function.

The rates of contraction, ATP utilization, and oxygen consumption in the myocardium all vary about three- to five-fold from resting conditions to strenuous exertion in the healthy mammalian heart. ATP to drive contraction, ion handling and other processes, is generated to match demand over this range of work, primarily by mitochondrial oxidative ATP synthesis [21,10](Bass and Vinnak2004; Bass 2008). This variation persists in spite of the fact that all the cardiomyocytes are activated each beat as excitation spreads over the whole heart. Cardiac action potential generation is probably the best characterized integrated cellular phenomena [92,93](Noble1962, 2012); while ATP is required for regaining ionic balance after each beat, this component of ATP usage is smaller and probably more uniform than is the consumption for force development.

A long-term imbalance over months to years between the force of contraction demanded for function and the ability of the cardiomyocytes to generate the contractile force needed can lead to failure. In the short-term cardiac metabolism changes between rest and exercise, using relatively more glucose at higher levels of work. For example in cardiac dyssynchrony, as occurs in left bundle branch block, LBBB, or pacing from the right ventricular outflow tract [122](van Oosterhout 2002), the metabolism changes toward a lower work state in the septum and toward a high work state in the LV free wall. The reason for this is that the early septal activation results in a rapid contraction since there is almost no load to oppose septal fiber shortening; this contraction stretches the not-yet-activated fibers in the lateral free wall opposite the septum before it contracts. About a hundred milliseconds later the now-activated free wall begins a longer, strongly preloaded contraction. Continued dyssynchrony of this sort results in remodeling of the heart. (A relatively new treatment for LBBB is to use dual electrode stimulation, attempting to provide cardiac resynchronization by stimulating the late-activated part of the ventricle earlier than occurs with the slow spread of activation through the myocardium.)

Altehoefer [5](1998) reviewed early evidence that in LBBB there was reduction in flow and glucose uptake in the septum. We know also from the work of Eisner [48](Eisner 2005), for example, that glucose uptake is increased in the LV free wall and reduced in the early-activated septal wall. Thus glucose metabolism and local cardiac work diminish in the early-activated unloaded region, and both increase in the late-activated region. This situation is an ideal one to study for there is an inbuilt control: two regions with all the same conditions except for the timing of excitation and the load-time sequence. The regions have the same blood composition and the same cycle time. In normal dogs the uptake of fatty acid by the heart is in each region in virtually direct proportionately to flow [37](Caldwell94), and the proportionality factor is so high that the observation cannot be explained by simple membrane permeation but requires that uptake kinetics are relatively more facilitated in high flow regions. The mechanism is not clear, but the suggestion is strong that it is receptor or transporter mediated [89][Musters 2006]. Fatty acid uptake is not really slowed by hypoxia or ischemia, but its metabolism is slowed. The uptake of tracer-labeled fatty acid was used as

an early method of infarct hot-spot imaging because the tracer fatty was not metabolized but retained preferentially in the hypoxic regions [51,52][Evans 1963, 1965]

What is not known is the time course of the shifts in metabolism after initiation of LBBB. Kinetically, biochemical systems are designed for fast responses and require no changes in gene expression. Even inserting stored GLUT4 glucose transporters into cell membranes takes only minutes [109](Sedaghat 2002). One would like to know how long it takes for the glucose uptake shifts to occur, but we know from Prinzen [101](1990) and subsequent studies [e.g.[121,122] van Oosterhout, 1998, 2002] that the patterns of timing and strain are stable in a very few minutes after changing the activation pattern. Such changes should be evident by MR tagging [42,84](Clarysse,2000; Maier et al 1992) to show changes in strain both acutely and chronically or by ultrasound [47](D'Hooge 2000). Dogs paced asynchronously for 6 months at normal rates do not go into heart failure [122](van Oosterhout 2002), but there is massive remodeling, as measured by wall thickness, and it begins early, being measurable at the cellular level in hours and days after inducing either dyssynchrony or a regional infarction. See reviews by Swynghedauw[115] (1999) and by Spinale [112](2007).

Unlike in skeletal muscle, ATP utilization in the heart does not normally exceed the capacity for oxidative synthesis: ATP production rate is tightly synchronized with the ATP utilization rate *in vivo*. Early investigations into the control of oxidative phosphorylation pointed to ADP as the critical signal stimulating ATP production in a feedback mechanism where increasing rate of ATP utilization leads to build-up the hydrolysis product ADP, which in turn, stimulates mitochondrial uptake and phosphorylation of ADP [39,6][Chance 1956; Atkinson 1968]. Indeed, the theory of ADP-mediated feedback control in skeletal muscle has stood the test of time with the advent of ^{31}phosphate magnetic resonance spectroscopy (^{31}P-MRS) to assay phosphate metabolites in muscle *in vivo*. Using ^{31}P-MRS in experiments on human subjects thirty years after his pioneering *in vitro* studies, Chance et al. [40][1985] could confidently conclude that in skeletal muscle "the primary control" is "exerted by ADP." More recent studies built on and refined these concepts [69,123][Jeneson 96; Vicini 2000]. Yet, while the advent of ^{31}P-MRS technology facilitated clear progress in the field of skeletal muscle energetics by helping to validate and refine existing hypotheses and ruling out competing alternatives, the early *in vivo* ^{31}P-MRS measurements on heart could not be explained based on the same mechanism apparently at work in skeletal muscle. Specifically, experiments in animal models failed to show a measureable change in estimated ADP concentration in the myocardium over a range of work rates [7][Balaban 86]. These observations led to the establishment of the "metabolic" hypothesis that, in the heart, ATP hydrolysis products are maintained at constant levels and thus cannot facilitate feedback-mediated control of ATP synthesis *in vivo*. Since feedback is excluded as a primary controller, the metabolic stability hypothesis implicitly invoked open-loop control (through an unknown mechanism) as the primary mechanism.

More recent studies have excluded the metabolic stability hypothesis and pointed to inorganic phosphate (Pi) as a key feedback signal regulating oxidative phosphorylation in the heart *in vivo* [127,128,129,130,131,25,32,26,34] [Wu 2007a,2007b, 2008, 2009a, 2009b; Beard 2005a,b, 2006, 2008]. Indeed, going beyond demonstrating that Pi does vary *in vivo* in the myocardium over the range associated with stimulation of oxidative phosphorylation, Beard's group has attempted to quantify how much of the regulation could be accounted for by feedback, versus other mechanisms such as open-loop stimulation by calcium ion or other signals. We conclude that Pi-mediated feedback not merely contributes, but probably dominates the control *in vivo*. The conclusion from the computational modeling showed that when calcium-mediated control is left out of simulations of oxidative phosphorylation, the *in vivo* data are reproduced, and thus any potential additional calcium-mediated effect must be small compared to the feedback mechanism. This finding is demonstrated by what is

perhaps the simplest extant model of oxidative phosphorylation that can predict the experimental data [27][Beard 2011], illustrated in Figure 9. Additional independent tests of the alternative hypothesis that change calcium levels can stimulate oxidative phosphorylation reveal that over the expected *in vivo* range of calcium concentration demonstrate that calcium modulation of mitochondrial dehydrogenase activity cannot provide adequate stimulation of mitochondrial oxidative phosphorylation to serve as an open-loop control mechanism of oxidative phosphorylation in the heart [124][Vinnakota et al 2011].

While a solid theoretic understanding (and associated computational models) of mitochondrial energy metabolism, and particularly of oxidative phosphorylation, in the heart has emerged in recent years, the overall picture of substrate utilization in the heart is not completely understood. The heart is capable of utilizing both carbohydrates and fatty acids to maintain phosphorylation potential necessary to sustain function under various physiological conditions. Randle [103][1998] proposed a conceptual model for the interactions between glucose and fatty acid utilization wherein each substrate inhibits the utilization of the other. One of the component mechanisms is the inhibition of phosphofructokinase and the consequent diminished fraction of glycolytic flux that enters the citrate acid cycle. The more modern refinement is yet more complex, but still not completely clear, as seen for example in the nice isotopomer studies by Metallo et al [87](2012) relating the shifts in use of glucose, fatty acid and glutamine that occur with hypoxia. Glutamine itself makes a contribution to maintaining energy balance even while supplying AcylCoA that is used for fatty acid formation and incorporation into membrane lipid.

Garfinkel and coworkers [1,2,3,76,77,78][Achs 68, 77, 82; Kohn 79, 83a,83b] pioneered the development of computational models of glucose and fatty acid utilization in the heart, based on catalytic mechanisms of the enzymes in those pathways. The primary aim of their studies was to explain the observed experimental behavior of metabolite concentrations on the basis of enzyme kinetic mechanisms that were used to describe the reaction fluxes, which constituted their working hypotheses. For example, their simulation of palmitate metabolism in perfused hearts led to the conclusion that citrate did not inhibit glycolysis, simply because citrate is mainly in the mitochondria not the cytosol where glycolysis occurs [77,78][Kohn 83a,b]. At the same time, their model was interpreted to be consistent with the creatine kinase shuttle concept for intracellular fluxes of high energy phosphate from sources to sinks inside the cell, whereas an alternative hypothesis treating the creatine kinase reaction at equilibrium could explain data on phosphoenergetics in the intact working heart [127,131][Wu 2008, 2009a].

Kroll and colleagues[80] have measured and modeled myocardial phosphoenergetics in perfused rabbit hearts with normal perfusion and during underperfusion showing how well the phosphorylation potential is maintained with the system buffering by PCr. Later work from this lab showed that repeated underperfusion, like preconditioning, led to downregulation of AMP hydrolysis. Recent modeling of whole heart metabolism by Zhou et al. [136,137,138][2005, 2006, 2007] have utilized phenomenological approaches for describing substrate utilization and phosphoenergetics to analyze limited data from perfused hearts. Zhou et al's model analyses required the hypothetical parallel activation wherein multiple enzymatic fluxes including those of mitochondrial electron transport chain are modulated simultaneously in response to demand in an open loop manner [137][Zhou 2006]. However, the existence of such control in mitochondrial electron transport and phosphorylation is contradicted by the arguments of Beard and coworkers [27][2011]. This illustrates the difficulty in mechanistic interpretation when data of several types such as intermediate metabolite concentrations from chemical measurements, blood flow and oxygen

consumption and phosphate metabolite data from NMR spectroscopy from comparable experiments are either not available or are not analyzed with appropriate theoretical models.

A reasonable strategy for tackling the problem of substrate utilization might necessitate the use of constraint-based methods, where one could identify sites of enzymatic regulation between different modes of operation [32][Beard and Qian, 2005]. Constraint-based analysis uses physicochemical principles combined with the specific experimental data to define limits to the particular arrangement of fluxes to provide an objective function (e.g., maximization of ATP generation flux). Detailed kinetic models with appropriately designed experiments are useful in investigating the kinetic and molecular bases of the predicted regulatory sites. These will necessarily be complex, as they must account for multiple cell types, e.g. the different influences of endothelial and muscle cells in purine transport[107].

SECTION V. Regional cardiac work and its measurement

The work of the heart is usually measured globally as “external work”, for example as cardiac output times systolic pressure, or the heart rate times the integral of the flow-pressure product over the time when the aortic valve is open, or less formally as heart rate times the maximum rate of rise of left ventricular pressure. Because myocardial cells and fibroblasts form a syncytium via intercellular gap-junctional connections [105][Sachse 08], the cells are activated almost in synchrony as the excitation spreads throughout the heart; this has given rise to the false notion that all cells work equally hard. While it is reasonable to believe that the rates of ATP use for cell maintenance and ion pumping (to maintain the cytosolic ionic milieu) might be similar throughout the heart, the data on regional myocardial blood flows prove that cardiac oxygen use and ATP turnover cannot be uniform. The evidence is clear: the low flow regions of the heart do not receive enough oxygen to sustain an average oxygen consumption for the heart, therefore the ATP turnover in these regions has to be less than average for the heart [74][King89]. The longer action potential duration in endocardial regions has long been recognized [95][Pandit2001]; put together with the observation that the subendocardial regions are especially vulnerable to infarction, one might have expected the subendocardium to have lower blood flows, but this is not borne out by the data. Endocardial flows in the normal heart are the same as the average for the heart. The low flow regions are scattered throughout the heart, and in a given heart remain consistently lower than average despite changes in the mean flows [74,75][King85, 89].

Regional strain, stress and work have been estimated mathematically through the use of detailed finite element models of cardiac function [90,118,117][Nickerson05; Usyk03; Trayanova11]. However the validity of local model-based estimates of work has not been tested against local measurements of tension and stress [91][Niederer09]. More detailed measurements can be obtained on local strains from tagged MRI and ultrasound images [84,42,47][Maier 92 Clarysse 00; D’Hooge00]; the question is how to infer from these the local stress and work. The difficulty is that calculating the local stress from local strain requires assumptions about dynamic tissue properties in the local and the neighboring regions in the complex 3D geometry, a process fraught with error, but probably achievable. Parameterizing models having regional contractile performance, so that local strain and stress are outputs of the computation, to match the detailed data on strain patterns is an alternative approach. This is computationally expensive for it requires the detailed anatomy of fiber and sheet arrangements as well as accurate MRI- or X-ray-CT strain data. Since there will be many outputs from the model, local strain measurements, the overall cardiac shapes and the ventricular volumes, pressures, and flows, the estimates of stress will be relatively constrained and should be meaningful. The end result should allow local work to be estimated for comparison with blood flow measurements (microspheres or MRI contrast agents) and perhaps Positron Emission Tomographic estimates of oxygen consumption.

These kinds of observations would provide large amounts of data on statistical associations among local flows, strain and work, and oxygen uptake.

To take the question a level deeper, one needs to incorporate into the 3-D models the particular hypothesized relationships between local work, ATP consumption and oxygen consumption, preferably at first in steady state situations. To start with, simple mechanistically based computational models of stress and strain development in sarcomeres in series have been used to represent asynchronous activation [10][Bassingthwaighte 08]. See Figure 10. This is analogous to left bundle branch block, LBBB, and the temporal asynchrony in cardiac excitation. The two elements represent the early- and late-activated portions of the LV, arranged in tandem so that each pulls upon the other. The early septal contraction stretches the free wall segments prior to their activation, so in accord with the Frank-Starling law the free wall generates extra force, and maintains cardiac output. The greater initial length of the prestretched segment leads to unequal regional force generation. The model mimics the relationships among shortening strain, strain velocity, stress, and ATP consumption. The link between the contractile events and regional flow would presumably be mediated through local metabolic demands, consumption of substrates and oxygen used to form ATP.

The hydrolysis of ATP at the cross-bridge drives the utilization of substrates and oxygen that supply the ATP. The model result in Figure 10 showed that the ATP use is over 10% higher in the late activated region. We have chosen, for simplicity, to use the stoichiometric kinetic model of van Beek [120][2007] that is based on the idea that the ADP levels in the cytosol and in the mitochondrial intermembrane space are the primary drivers for mitochondrial ATP generation. Beard's [25][2005a] is the best detailed model for mitochondrial oxidative phosphorylation. Though our premise lacks Beard's mechanistic biochemical detail, the two-muscles-in-series model qualitatively defines the rate of conversion of ATP to ADP and the resultant ADP levels to drive O_2 demand. At high workloads there is release of adenosine into the interstitial space, activating A_2 receptors and inducing smooth muscle vasodilatation. The inference is that in regions where there is high demand there is, at least transiently, sufficient ATP breakdown in excess of the mitochondrial capacity for the phosphorylation of ADP to provide a vasodilatory signal. The vasodilatory response to interstitial adenosine is ultrasensitive [113][Stepp96], that is, the increase in coronary blood flow per unit adenosine concentration is switch-like, having a Hill coefficient of nearly 7.

This type of model can be extended to represent temporal asynchronous activation of sarcomeres or fiber bundles in series and in parallel to represent a 2D slice of the ventricular wall. Models of higher complexity must take the 3D muscle fiber orientation into account. Models at this intermediate level of complexity could be parameterized to data in a computationally tractable manner to provide a step toward validating models of cardiac stress, strain and work to experimental measurements.

With cardiac systole the increased tissue pressure, effectively the extravascular pressure, acts to compress coronary vessels, slowing or even reversing arterial inflow and markedly enhancing venous outflow. Since flow usually reverses in the early phase of systole in the LAD, for example, this implies a major increase in resistance and a decrease in the vessel sizes within the transmural segments, presumably due to compression by flattening them. While Vis and Westerhof [125][Vis97] showed that compression of the venae comitantes, the pair of venules accompanying each arteriole, can provide some protection against the arteriolar compression, the flow reversal is nevertheless present. The increased pressure is greatest in the LV endocardium and is a reason for the higher incidence of subendocardial infarctions. Algranati et al. [4][Algranati 2010] have described this myocardium-vessel

interaction effect as shown in Figure 11. Gorman and Feigl [57][Gorman2012] feel that arteriolar α-adreno receptors upstream are activated during increased workload in an effort to minimize the reduction in arterial flow during systole and to reestablish flow immediately after each systole. These vascular regulatory effects coupled with the well established response of the vasculature to intraluminal pressure, flow-induced shear on the vessel wall and metabolic signals conducted upstream from regions of low oxyhemoglobin saturation in the venules [57,49](Gorman2012; Ellsworth2009] will provide insights into how regional blood flow heterogeneity can be related to regional stress, strain and work.

When LBBB is initiated the strain, stress and work, are changed locally, not globally. The remodeling of the vascular system and the cardiac muscle are probably activated simultaneously. Mechanical stress is decreased in the septum, increased in late activated regions, and remains normal in regions in between. Estimating stress levels at millimeter resolution of fiber bundle and sheet structure in heart will be needed to interpret the similarly high-resolution data on regional flows and work. Dissection methods may be required for fiber direction if Diffusion Tensor Imaging (DTI) *in vivo* cannot provide sufficient spatial resolution. Likewise, the spatial resolution in current techniques for measuring regional flows or strain measurements in 3D heart using MRI is at the edge of practicability.

The mechanics of cardiac contraction begins with actin/myosin interactions at the cross-bridge, when contractile force is developed in the presence of Ca^{2+}-binding to troponin. The kinetics of the events leading to myofilament shortening were demonstrated for skeletal muscle and provided with a prescient hypothetical explanation by Huxley [68](1957). The recent explanations take into account the several different myofilament proteins and their interactions [116](Tanner et al 2008) and extend the details to account for the Starling effect, that lengthening the fibers prior to contraction produces a stronger contraction [111][Smith et al 2009], whose model accounts for the amount of ATP hydrolysis, as was attempted in the earlier models of Landesberg and Sideman [81][1994].

SECTION VI. Tracking the relationships from organ to genome

What more is needed to demonstrate that regional stress and work actually provide the drive for regional metabolism and remodeling of the musculature and of the vascular system serving the muscle cells? What are the mechanisms by which this might occur? How should we approach determining the cause-and-effect relationships? These nagging questions remain. From the point of view of capturing a systematic quantitative understanding of the mechanisms of cell maintenance and of the remodeling that follows modification of behavior or the disorder of disease, one tends to be “cell-centric”. This is the “middle out” approach to understanding the biology that we recommend as a central strategy for the Physiome Projects [19][Bassing, NobleHunter09]. “Middle out” implies that we should start at the cell level where we have the most quantitative data and many integrative model descriptions of those data; from the cell we can work “upward” to tissue, organ and organism, and “downward” to subcellular systems, the proteome, transcriptome and genome. From the point of view of normal physiological remodeling it is the modulation of the transcriptome that is central: this means undertaking a cell-to-genome approach.

A top down, cell-to-genome, approach is quite the opposite of the strategy of many molecular biologists. Their emphasis has been on a bottom up approach, finding associations in mRNA and protein profiles, the transcriptome and the proteome, in order to define the pathways for synthesis, proteolysis, and regulation of fluxes. But proteolysis, or autophagy, cleaning out old proteins and recycling their amino acids, is just as important as manufacturing proteins [41][Ciechanover, 2012]. Generalized autophagy is stimulated by

exercise [60][He 2012] and is probably one of the reasons that exercise regimens prolong life. Genes for proteases are therefore as beneficial as genes for structural and enzymic proteins. In general, the robustness of the body's responses to perturbations is centered at the cell level, and the responses to stresses are brought about via regulation at the cell level.

Changes in transcription rates are initiated indirectly by high-level directives, from the brain or from the environment. The mind says, "start exercising". Exercise training builds more contractile machinery into cells. The intracellular response to the increased workload is signaled down to the gene: at the nuclear level the rates of transcription of particular proteins are increased. A particular chromosome is uncoiled and a particular region becomes the site of ribosomal activity. The response is not general; it only occurs in muscle cells doing extra work. The signaling and the response are at the cell level. Thus to determine how the cell is signaling to a particular part of the genome is a real puzzle.

It is easier to track the response. In the particular case of myofilament production, one would track the gene products or transcriptome for actin and myosin (and other components of the contractile apparatus). The general principle is to provoke the cell in a highly specific manner so as to get the most narrowly defined response, and then to characterize that response. Proteomic techniques, such as following the time course of new myosin formation along with other proteins changing in coordinated fashion, should help to define the pathway from transcription to installation as part of a sarcomere. Presumably as the muscle building reaches steady state the levels of the signals diminish. On this basis one would look for components of the metabolome, substrates or analytes or proteins that rise when the exercise training starts and diminish when steady state is reached, and do the opposite when training is suddenly stopped. Careful attention to the timing of responses should augment the power of the Boolean inference engines used in proteomic searches for correlations.

CONCLUSION

Cardiac electrophysiological modeling, from cell to organ, has been rather well defined through the detailed biophysical measurements and analyses made over the last 5 decades since Noble's [92,93](1962, 2012) pioneering initiation of the field. This particular field is probably the most precisely determined set of physiological processes; it sets a standard for quality and depth in the analysis in terms of model representation. Modeling is developing well for cardiac mechanics, from the point of view of myofilament interactions, where the emphasis now is on the combination of the biophysics and biochemistry providing force generation. The modeling appears accomplishable for energetics and biochemical processes as the data accumulates and the hypotheses are expressed in ever more complete forms. All of these are related to, or governing, the heterogeneities in flows in the heart. Biochemical events will be to some extent identifiable in intact hearts using optical probes. It is in the conceptual integrating and practical modeling that the advances occur in specific experimental or analytical studies [31](Beard and Kushmerick 2009) or in the all embracing strategies guiding the Physiome Projects [19](Bass, Noble Hunter 2009), where major successes are occurring to link cell, organ and systems behavior. On the other hand cell-to-gene regulation is poorly defined, and signaling pathways are still difficult to identify, let along quantitate. The gene-to-cell to phenotype is being explored and beginning to be uncovered through statistical inference methods, but the complexity of the system and the low statistical resolution in defining network structure and topology makes progress slow. Identifying the signaling pathways for regulating transcription and autophagy appear to be the big hurdles. Nevertheless the cardiac Physiome is clearly accomplishable, but it will be a long adventure.

Acknowledgments

The authors thank Erik Butterworth for his development of JSim and its archival forms in XMML, Lucian Smith and Erik B. for their development of translators to and from JSim to SBML and Cell ML. Gary Raymond and Bartholomew Jardine for coding and curation of many of these models, and for making the models available to readers at: www.physiome.org.

The models and the Simulation Analysis System JSim are free to be downloaded and run on any Linux, Macintosh OSX, or Windows platform. Research was supported by NIH grants NHLBI T32 HL7403, T15 088516, and R01 HL19139, NIBIB R01 EB01973, R01 EB08407, and NIGMS 1-P50-GM094503.

References

1. Achs MJ, Garfinkel D. Simulation of the detailed regulation of glycolytic oscillation in a heart supernatant preparation. Computers and Biomedical Research. 1968; 2:92–110. [PubMed: 4247123]
2. Achs MJ, Garfinkel D. Computer simulation of rat heart metabolism after adding glucose to the perfusate. Am J Physiol Regulatory Integrative Comp Physiol. 1977; 232:R175–184.
3. Achs MJ, Garfinkel D. Computer simulation of energy metabolism in acidotic cardiac ischemia. Am J Physiol Regulatory Integrative Comp Physiol. 1982; 242:R533–544.
4. Algranati D, Kassab GS, Lanir Y. Mechanisms of myocardium-coronary vessel interaction. Am J Physiol Heart Circ Physiol. 2010; 298:H861–H873. [PubMed: 19966048]
5. Altehoefer C. Editorial: LBBB: Challenging our concept of metabolic heart imaging with fluorine-18-FDG and PET. J Nucl Med. 1998; 39:263–265. [PubMed: 9476933]
6. Atkinson DE. The energy charge of the adenylate pool as a regulatory parameter. Interaction with feedback modifiers. Biochemistry. 1968; 7(11):4030–4034. [PubMed: 4972613]
7. Balaban RS, et al. Relation between work and phosphate metabolite in the *in vivo* paced mammalian heart. Science. 1986; 232(4754):1121–3. [PubMed: 3704638]
8. Bassingthwaighte JB. A concurrent flow model for extraction during transcapillary passage. Circ Res. 1974; 35:483–503. [PubMed: 4608628]
9. Bassingthwaighte JB. The modelling of a primitive ‘sustainable’ conservative cell. Phil Trans Roy Soc London A. 2001; 359:1055–1072.
10. Bassingthwaighte JB. Linking cellular energetics to local flow regulation in the heart. Ann New York Acad Sci. 2008; 1123:126–133. [PubMed: 18375585]
11. Bassingthwaighte JB, Beard DA. Fractal ^{15}O-water washout from the heart. Circ Res. 1995; 77:1212–1221. [PubMed: 7586234]
12. Bassingthwaighte JB, Beyer RP. Fractal correlation in heterogeneous systems. Physica D. 1991; 53:71–84.
13. Bassingthwaighte JB, Chan IS, Wang CY. Computationally efficient algorithms for capillary convection-permeation-diffusion models for blood-tissue exchange. Ann Biomed Eng. 1992; 20:687–725. [PubMed: 1449234]
14. Bassingthwaighte, JB.; Dobbs, WA.; Yipintsoi, T. Heterogeneity of myocardial blood flow. In: Maseri, A., editor. Myocardial Blood Flow in Man: Methods and significance in coronary disease. Torino, Italy: Minerva Medica; 1972. p. 197-205.
15. Bassingthwaighte, JB.; Goresky, CA. Modeling in the analysis of solute and water exchange in the microvasculature. In: Renkin, EM.; Michel, CC., editors. Handbook of Physiology. Sect. 2, The Cardiovascular System. Vol IV, The Microcirculation. Am. Physiol. Soc; Bethesda, MD: 1984. p. 549-626.1.
16. Bassingthwaighte JB, King RB, Roger SA. Fractal nature of regional myocardial blood flow heterogeneity. Circ Res. 1989; 65:578–590. [PubMed: 2766485]
17. Bassingthwaighte, JB.; Liebovitch, L.; West, BJ. Fractal Physiology. Oxford University Press; 1994. p. 364
18. Bassingthwaighte JB, Malone MA, Moffett TC, King RB, Little SE, Link JM, Krohn KA. Validity of microsphere depositions for regional myocardial flows. Am J Physiol Heart Circ Physiol. 1987; 253:H184–H193.

19. Bassingthwaighte JB, Noble D, Hunter PJ. The Cardiac Physiome: perspectives for the future. Experimental Physiology. 2009; 94.5:597–605. [PubMed: 19098089]
20. Bassingthwaighte JB, van Beek JHGM. Lightning and the heart: fractal behavior in cardiac function. Proc IEEE. 1988; 76(6):693–699.
21. Bassingthwaighte, JB.; Vinnakota, KC. The computational integrated myocyte. A view into the virtual heart. In: Sideman, S.; Beyar, R., editors. Modeling in Cardiovascular Systems. Vol. 1015. Ann. New York Acad. Sci; 2004. p. 391-404.
22. Bassingthwaighte JB, Wang CY, Chan IS. Blood-tissue exchange via transport and transformation by endothelial cells. Circ Res. 1989; 65:997–1020. [PubMed: 2791233]
23. Bassingthwaighte JB, Yipintsoi T, Harvey RB. Microvasculature of the dog left ventricular myocardium. Microvasc Res. 1974; 7:229–249. [PubMed: 4596001]
24. Beard DA. Computational framework for generating transport models from databases of microvascular anatomy. Ann Biomed Eng. 2001b; 29:837–843. [PubMed: 11764314]
25. Beard DA. A biophysical model of the mitochondrial respiratory system and oxidative phosphorylation. PLoS Comput Biol. 2005a; 1(4):e36. [PubMed: 16163394]
26. Beard DA. Modeling of oxygen transport and cellular energetics explains observations on *in vivo* cardiac energy metabolism. PLoS Comput Biol. 2006; 2(9):e107. [PubMed: 16978045]
27. Beard DA. Simulation of cellular biochemical system kinetics. Wiley Interdiscip Rev Syst Biol Med. 2011; 3(2):136–46. [PubMed: 21171044]
28. Beard DA, Bassingthwaighte JB. The fractal nature of myocardial blood flow emerges from a whole-organ model of arterial network. J Vasc Res. 2000a; 37:282–296. [PubMed: 10965227]
29. Beard DA, Bassingthwaighte JB. Advection and diffusion of substances in biological tissues with complex vascular networks. Ann Biomed Eng. 2000b; 28:253–268. [PubMed: 10784090]
30. Beard DA, Bassingthwaighte JB. Modeling advection and diffusion of oxygen in complex vascular networks. Ann Biomed Eng. 2001a; 29:298–310. [PubMed: 11339327]
31. Beard DA, Kushmerick MJ. Strong inference for systems biology. PLoS Comput Biol. 2009; 5(8):e1000459. [PubMed: 19714210]
32. Beard DA, Qian H. Thermodynamic-based computational profiling of cellular regulatory control in hepatocyte metabolism. Am J Physiol Endocr Metab. 2005b; 288(3):E633–44.
33. Beard DA, KA, Schenkman EO. Feigl, Myocardial oxygenation in isolated hearts predicted by an anatomically realistic microvascular transport model. Am J Physiol Heart Circ Physiol. 2003; 285:H1826–1836. [PubMed: 12869375]
34. Beard DA, Wu FME, Cabrera RK. Dash, Modeling of Cellular Metabolism and Microcirculatory Transport. Microcirculation. 2008; 15:777–793. [PubMed: 18608987]
35. Beyer RP Jr, Bassingthwaighte JB, Deussen AJ. A computational model of oxygen transport from red blood cells to mitochondria. Comput Methods Programs Biomed. 2002; 67:39–54. [PubMed: 11750946]
36. Buerk DG, Bridges EW. A simplified algorithm for computing the variation in oxyhemoglobin saturation with pH, PCO2, T and DPG. Chem Eng Commun. 1986; 47:113–124.
37. Caldwell JH, Martin GV, Raymond GM, Bassingthwaighte JB. Regional myocardial flow and capillary permeability-surface area products are nearly proportional. Am J Physiol Heart Circ Physiol. 1994; 267:H654–H666.
38. Cannon MJ, Percival DB, Caccia DC, Raymond GM, Bassingthwaighte JB. Evaluating scaled windowed variance methods for estimating the Hurst coefficient of time series. Physica A. 1997; 241:606–626. [PubMed: 22049250]
39. Chance B, Williams GR. The respiratory chain and oxidative phosphorylation. Adv Enzymol Relat Subj Biochem. 1956; 17:65–134. [PubMed: 13313307]
40. Chance B, Leigh JS, Clark BJ, Maris J, Kent J, Nioka S, Smith D. Control of oxidative metabolism and oxygen delivery in human skeletal muscle: a steady-state analysis of the work/energy cost transfer function. Proc Natl Acad Sci USA. 1985; 82:8384–8388. [PubMed: 3866229]
41. Ciechanover A. Intracellular Protein Degradation: From a Vague Idea through the Lysosome and the Ubiquitin-Proteasome System and onto Human Diseases and Drug Targeting. Ramban Maimonides Med J. 2012; 3:1–20.

42. Clarysse P, et al. Two-dimensional spatial and temporal displacement and deformation field fitting from cardiac magnetic resonance tagging. Medical Image Analysis. 2000; 4(3):253–268. [PubMed: 11145312]
43. Dash RK, Bassingthwaighte JB. Blood HbO2 and HbCO2 dissociation curves at varied O2, CO2, pH, 2,3-DPG and temperature levels. Ann Biomed Eng. 2004; 32:1676–1693. [PubMed: 15682524]
44. Dash RK, Bassingthwaighte JB. Simultaneous blood-tissue exchange of oxygen, carbon dioxide, bicarbonate, and hydrogen ion. Ann Biomed Eng. 2006; 34:1129–1148. [PubMed: 16775761]
45. Dash RK, Bassingthwaighte JB. Erratum to: Blood HbO2 and HbCO2 dissociation curves at varied O2, CO2, pH, 2,3-DPG and temperature levels. Ann Biomed Eng. 2010; 38:1683–1701. [PubMed: 20162361]
46. Deussen A, Bassingthwaighte JB. Modeling 15O-oxygen tracer data for estimating oxygen consumption. Am J Physiol. 1996; 270:H1115–1130. [PubMed: 8780210]
47. D'Hooge J, et al. Regional strain and strain rate measurements by cardiac ultrasound: principles, implementation and limitations. Europ J Echocardiography. 2000; 1(3):154–170.
48. Eisner RL, Meyer T, Sigman S, Eder S, Streeter J, Patterson R. Comparison of Contrast Enhanced Magnetic Resonance Imaging to Positron Emission Tomography with F-18 Fluorodeoxyglucose and Rb-82 for the Detection of Myocardial Viability Using Left Ventricular Bullseye Analysis. J Cardiovasc Magn Reson. 2005; 1:70–71. (Abstr.).
49. Ellsworth ML, Ellis CG, Goldman D, Stephenson AH, Dietrich HH, Spraque RS. Erythrocytes: oxygen sensors and modulators of vascular tone. Physiology. 2009; 24(2):107–116. [PubMed: 19364913]
50. Evans CL, Matsuoka Y. The effect of various mechanical conditions on the gaseous metabolism of the mammalian heart. J Physiol (Lond). 1915; 49:378–405. [PubMed: 16993302]
51. Evans JR, Opie LH, Shipp JL. Metabolism of palmitic acid in perfused rat heart. Am J Physiol. 1963; 205:766–770. [PubMed: 14060819]
52. Evans JR, Gunton RW, Baker RG, Beanlands DS, Spears JC. Use of radioiodinated fatty acid for photoscans of the heart. Circ Res. 1965; 16:1–10. [PubMed: 14252152]
53. Federspiel WJ, Popel AS. A theoretical analysis of the effect of the particulate nature of blood on oxygen release in capillaries. Microvascular Research. 1986; 32:164–189. [PubMed: 3762425]
54. Geers C, Gros G. Carbon dioxide transport and carbonic anhydrase in blood and muscle. Physiol Rev. 2000; 80:681–715. [PubMed: 10747205]
55. Glenny RW, Bernard S, Brinkley M. Validation of fluorescent-labeled microspheres for measurement of regional organ perfusion. J Appl Physiol. 1993; 74:2585–2597. [PubMed: 8335595]
56. Goldman D, Popel AS. A computational study of the effect of capillary network anastomoses and tortuosity on oxygen transport. J Theor Biol. 2000; 206:181–194. [PubMed: 10966756]
57. Gorman MW, Feigl EO. Control of coronary blood flow during exercise. Exercise and Sport Sciences Reviews. 2012; 40:37–42. [PubMed: 21918457]
58. Groebe K. A versatile model of steady state O2 supply to tissue. Application to skeletal muscle. Biophys J. 1990; 57:485–498. [PubMed: 2306498]
59. Groebe K, Thews G. Calculated intra- and extracellular PO2 gradients in heavily working red muscle. Am J Physiol. 1990; 259:H84–H92. [PubMed: 2375415]
60. He C, Bassik MC, Moresi V, Sun K, Wei Y, Zou Z, An Z, Loh J, Fisher J, Sun Q, Korsmeyer S, Packer M, May HI, Hill JA, Virgin HW, Gilpin C, Xiao G, Bassel-Duby R, Scherer PE, Levine B. Exercise-induced BCL2-regulated autophagy is required for muscle glucose homeostasis. Nature. 2012; 481:511–515. [PubMed: 22258505]
61. Hellums JD, Nair PK, Huang NS, Ohshima N. Simulation of intraluminal gas transport processes in the microcirculation. Ann Biomed Eng. 1996; 24:1–24. [PubMed: 8669708]
62. Hill EP, Power GG, Longo LD. A mathematical model of carbon dioxide transfer in the placenta and its interaction with oxygen. Am J Physiol. 1973a; 224:283–299. [PubMed: 4686484]
63. Hill EP, Power GG, Longo LD. Mathematical simulation of pulmonary O2 and CO2 exchange. Am J Physiol. 1973b; 224:904–917. [PubMed: 4698808]

64. Hofmeyr J-HS, Cornish-Bowden A. The reversible Hill equation: How to incorporate cooperative enzymes into metabolic models. Comput Appl Biosci. 1997; 13:377–385. [PubMed: 9283752]
65. Huang NS, Hellums JD. A theoretical model for gas transport and acid/base regulation by blood flowing in microvessels. Microvasc Res. 1994; 48:364–388. [PubMed: 7731399]
66. Huang SC, Feng DG, Phelps ME. Model dependency and estimation reliability in measurement of cerebral oxygen utilization rate with oxygen-15 and dynamic positron emission tomography. J Cereb Blood Flow Metabol. 1986; 6:105–119.
67. Hurst HE. Long-term storage capacity of reservoirs. Trans Amer Soc Civ Engrs. 1951; 116:770–808.
68. Huxley AF. Muscle structure and theories of contraction. Prog Biophys Biophys Chem. 1957; 7:255–318. [PubMed: 13485191]
69. Jeneson JAL, Wiseman RW, Westerhoff HV, Kushmerick MJ. The signal transduction function for oxidative phosphorylation is at least second order in ADP. J Biol Chem. 1996; 271(45):27995–27998. [PubMed: 8910406]
70. Kassab GS, Imoto K, White FC, Rider CA, Fung YCB, Bloor CM. Coronary arterial tree remodeling in right ventricular hypertrophy. Am J Physiol Heart Circ Physiol. 1993; 265:H366–H375.
71. Kelman GR. Digital computer subroutine for the conversion of oxygen tension into saturation. J Appl Physiol. 1966; 21:1375–1376. [PubMed: 5916678]
72. Kendal WS. A stochastic model for the self-similar heterogeneity of regional organ blood flow. Proc Nat Acad Sci. 2001; 98:837–841. [PubMed: 11158557]
73. Kettunen MI, Grohn OH, Silvennoinen MJ, Penttonen M, Kauppinen RA. Quantitative assessment of the balance between oxygen delivery and consumption in the rat brain after transient ischemia with T2 -BOLD magnetic resonance imaging. J Cereb Blood Flow Metab. 2002; 22:262–270. [PubMed: 11891431]
74. King RB, Bassingthwaighte JB, Hales JRS, Rowell LB. Stability of heterogeneity of myocardial blood flow in normal awake baboons. Circ Res. 1985; 57:285–295. [PubMed: 4017198]
75. King RB, Bassingthwaighte JB. Temporal fluctuations in regional myocardial flows. Pfluegers Arch (Eur J Physiol). 1989; 413/4:336–342. [PubMed: 2928084]
76. Kohn MC, Achs MJ, Garfinkel D. Computer simulation of metabolism in pyruvate-perfused rat heart. I. Model construction. Am J Physiol Regulatory Integrative Comp Physiol. 1979; 237:R153–158.
77. Kohn MC, Garfinkel D. Computer simulation of metabolism in palmitate-perfused rat heart. I. Palmitate oxidation. Ann Biomed Eng. 1983a; 11:361–384. [PubMed: 6592996]
78. Kohn MC, Garfinkel D. Computer simulation of metabolism in palmitate-perfused rat heart. II. Behavior of complete model. Ann Biomed Eng. 1983b; 11:511–531. [PubMed: 6391299]
79. Krogh A. The number and distribution of capillaries in muscle with calculations of the oxygen pressure head necessary for supplying the tissue. J Physiol (Lond). 1919; 52:409–415. [PubMed: 16993405]
80. Kroll K, Kinzie DJ, Gustafson LA. Open system kinetics of myocardial phosphoenergetics during coronary underperfusion. Am J Physiol Heart Circ Physiol. 1997; 272:H2563–H2576.
81. Landesberg A, Sideman S. Regulation of energy consumption in cardiac muscle: analysis of isometric contractions. Am J Physiol Heart Circ Physiol. 1999; 276:H998–H1011.
82. Li Z, Yipintsoi TJB. Bassingthwaighte, Nonlinear model for capillary-tissue oxygen transport and metabolism. Ann Biomed Eng. 1997; 25:604–619. [PubMed: 9236974]
83. Little SE, Bassingthwaighte JB. Plasma-soluble marker for intraorgan regional flows. Am J Physiol Heart Circ Physiol. 1983; 245:H707–H712.
84. Maier SE, et al. Evaluation of left ventricular segmental wall motion in hypertrophic cardiomyopathy with myocardial tagging. Circulation. 1992; 86:1919–1928. [PubMed: 1451263]
85. Mandelbrot BB, Van Ness JW. Fractional Brownian motions, fractional noises and applications. SIAM Rev. 1968; 10:422–437.

86. Marcus ML, Kerber RE, Erhardt JC, Falsetti HL, Davis DM, Abboud FM. Spatial and temporal heterogeneity of left ventricular perfusion in awake dogs. Am Heart J. 1977; 94:748–754. [PubMed: 920583]
87. Metallo CM, Gameiro PA, Bell EL, Mattaini KR, Yang J, Hiller K, Jewell CM, Johnson ZR, Irvine DJ, Guarante L, Kelleher JK, Vander Heiden MG, Iliopoulos O, Stephanopoulos G. Reductive glutamine metabolism by IDH1 mediates lipogenesis under hypoxia. Nature. 2012; 481:380–384. [PubMed: 22101433]
88. Mintun MA, Raichle ME, Martin WR, Herscovitch P. Brain oxygen utilization measured with O-15 radiotracers and positron emission tomography. J Nucl Med. 1984; 25:177–187. [PubMed: 6610032]
89. Musters MWJM, Bassingthwaighte JB, van Riel NAW, van der Vusse GJ. Computational evidence for protein-mediated fatty acid transport across the sarcolemma. Biochem J. 2006; 393:669–678. [PubMed: 16207175]
90. Nickerson D, Smith N, Hunter P. New developments in a strongly coupled cardiac electromechanical model. Europace. 2005; 7:S118–S127.3.
91. Niederer SA, Smith NP. The role of the Frank-Starling law in the transduction of cellular work to whole organ pump function: a computational modeling analysis. PLoS Computational Biology. 2009; 5(4):e1000371. [PubMed: 19390615]
92. Noble D. A modification of the Hodgkin-Huxley equations applicable to Purkinje fibre action and pace-make potentials. J Physiol. 1962; 160:317–352. [PubMed: 14480151]
93. Noble D, Garny A, Noble P. How the Hodgkin-Huxley equations inspired the Cardiac Physiome Project. J Physiol. 2012; 590:2613–2628. [PubMed: 22473779]
94. Ogawa S, Menon RS, Tank DW, Kim SG, Merkle H, Ellermann JM, Ugurbil K. Functional brain mapping by blood oxygenation level-dependent contrast magnetic resonance imaging. Acomparison of signal characteristics with a biophysical model. Biophys J. 1993; 64:803–812. [PubMed: 8386018]
95. Pandit SV, Clark RB, Giles WR, Demir SS. A mathematical model of action potential heterogeneity in adult left ventricular myocyte. Biophysical Journal. 2001; 81:3029–3051. [PubMed: 11720973]
96. Patterson SW, Piper H, Starling EH. The regulation of the heart beat. J Physiol. 1914; 48:465–513. [PubMed: 16993269]
97. Pekar J, Ligeti L, Ruttner Z, Lyon RC, Sinnwell TM, van Gelderen P, Fiat D, Moonen CT, McLaughlin AC. *In vivo* measurement of cerebral oxygen consumption and blood flow using 17O magnetic resonance imaging. Magn Reson Med. 1991; 21:313–319. [PubMed: 1745131]
98. Pekar J, Sinnwell T, Ligeti L, Chesnick AS, Frank JA, McLaughlin AC. Simultaneous measurement of cerebral oxygen consumption and blood flow using 17O and 19F magnetic resonance imaging. J Cereb Blood Flow Metab. 1995; 15:312–320. [PubMed: 7860664]
99. Popel AS. Theory of oxygen transport to tissue. Crit Rev Biomed Eng. 1989; 17:257–321. [PubMed: 2673661]
100. Pries AR, Secomb TW. Origins of heterogeneity in tissue perfusion and metabolism. Cardiovasc Res. 2009; 81:328–335. [PubMed: 19028725]
101. Prinzen FW, Augustijn CH, Arts T, Allessie MA, Reneman RS. Redistribution of myocardial fiber strain and blood flow by asynchronous activation. Am J Physiol (Heart Circ Physiol 28). 1990; 259:H300–H308.
102. Prinzen FW, Bassingthwaighte JB. Blood flow distributions by microsphere deposition methods. Cardiovasc Res. 2000; 45:13–21. [PubMed: 10728307]
103. Randle PJ. Regulatory interactions between lipids and carbohydrates: the glucose fatty acid cycle after 35 years. Diabetes/metabolism reviews. 1998; 14(4):263–283. [PubMed: 10095997]
104. Richmond DR, Tauxe WN, Bassingthwaighte JB. Albumin macroaggregates and measurements of regional blood flow: Validity and application of particle sizing by Coulter counter. J Lab Clin Med. 1970; 75:336–346. [PubMed: 5414411]
105. Sachse FB, Moreno A, Abildskov JA. Electrophysiological modeling of fibroblasts and their interaction with myocytes. Ann Biomed Eng. 2008; 36(1):41–56. [PubMed: 17999190]

106. Salathe EP, Fayad R, Schaffer SW. Mathematical analysis of carbon dioxide transfer by blood. Math Biosci. 1981; 57:109–153.
107. Schwartz LM, Bukowski TR, Revkin JH, Bassingthwaighte JB. Cardiac endothelial transport and metabolism of adenosine and inosine. Am J Physiol Heart Circ Physiol. 1999; 277:H1241–H1251.
108. Secomb TW, Hsu R, Beamer NB, Coull BM. Theoretical simulation of oxygen transport to brain by networks of microvessels: effects of oxygen supply and demand on tissue hypoxia. Microcirculation. 2000; 7:237–247. [PubMed: 10963629]
109. Sedaghat AR, Sherman A, Quon MJ. A mathematical model of metabolic insulin signaling pathways. Am J Physiol Endocrinol Metab. 2002; 283:E1084–E1101. [PubMed: 12376338]
110. Severinghaus JW. Simple, accurate equations for human blood O2 dissociation computations. J Appl Physiol. 1979; 46:599–602. [PubMed: 35496]
111. Smith L, Tainter C, Regnier M, Martyn DA. Cooperative crossbridge activation of thin filaments contributes to the Frank-Starling mechanism in cardiac muscle. Biophys J. 2009; 96:3692–3702. [PubMed: 19413974]
112. Spinale FG. Myocardial Matrix Remodeling and the Matrix Metalloproteinases: Influence on Cardiac Form and Function. Physiol Rev. 2007; 87:1285–1342. [PubMed: 17928585]
113. Stepp DW, Van Bibber R, Kroll K, Feigl EO. Quantitative relation between interstitial adenosine concentration and coronary blood flow. Circ Res. 1996; 79:601–610. [PubMed: 8781493]
114. Sutcliffe JV. Harold Edwin Hurst. Obituary Hydrology Sciences Bulletin. 1979; 24(4):539–541.
115. Swynghedauw B. Molecular Mechanisms of Myocardial Remodeling. Physiol Rev. 1999; 79:215–262. [PubMed: 9922372]
116. Tanner BCW, Regnier M, Daniel TL. A spatially-explicit model of muscle contraction explains a relationship between activation phase, power, and ATP utilization in insect flight. J Exp Biol. 2008; 211:180–186. [PubMed: 18165245]
117. Trayanova NA. Whole-heart modeling applications to cardiac electrophysiology and electromechanics. Circulation Res. 2011; 108(1):113–128. [PubMed: 21212393]
118. Usyk TP, McCulloch AD. Relationship between regional shortening and asynchronous electrical activation in a three-dimensional model of ventricular electromechanics. J Cardiovasc Electrophysiol. 2003; 14(10):S196–S202. [PubMed: 14760924]
119. van Beek JHGM, Roger SA, Bassingthwaighte JB. Regional myocardial flow heterogeneity explained with fractal networks. Am J Physiol Heart Circ Physiol. 1989; 257:H1670–H1680.
120. van Beek JHGM. Adenine nucleotide-creatine-phosphate module in myocardial metabolic system explains fast phase of dynamic regulation of oxidative phosphorylation. Am J Physiol Cell Physiol. 2007; 293:C815–C829. [PubMed: 17581855]
121. van Oosterhout MFM, Prinzen FW, Sakurada S, Glenny RW, Hales JRS. Fluorescent microspheres are superior to radioactive microspheres in chronic blood flow measurements. Am J Physiol Heart Circ Physiol. 1998; 275:H110–H115.
122. van Oosterhout MF, Arts T, Bassingthwaighte JB, Reneman RS, Prinzen FW. Relation between local myocardial growth and blood flow during chronic ventricular pacing. Cardiovasc Res. 2002; 53:831–840. [PubMed: 11922893]
123. Vicini P, Kushmerick MJ. Cellular energetics analysis by a mathematical model of energy balance: Estimation of parameters in human skeletal muscle. Am J Physiol Cell Physiol. 2000; 279:C213–C224. [PubMed: 10898733]
124. Vinnakota KC, Dash RK, Beard DA. Stimulatory Effects of Calcium on Respiration and NAD(P)H Synthesis in Intact Rat Heart Mitochondria Utilizing Physiological Synthesis in Intact Rat Heart Mitochondria Utilizing Physiological Substrates Cannot Explain Respiratory Control *in Vivo*. J Biol Chem. 2011; 286:30816–30822. [PubMed: 21757763]
125. Vis MA, Bovendeerd PH, Sipkema P, Westerhof N. Effect of ventricular contraction, pressure, and wall stretch on vessels at different locations in the wall. Am J Physiol Heart Circ. 1997; 272:H2963–H2975.
126. Winslow RM, Samaja M, Winslow NJ, Rossi-Bernardi L, Shrager RI. Simulation of continuous blood O2 equilibrium over physiological pH, DPG, and PCO2 range. J Appl Physiol. 1983; 54:524–529. [PubMed: 6403493]

127. Wu F, Beard DA. Roles of the creatine kinase system and myoglobin in maintaining energetic state in the working heart. BMC Syst Biol. 2009a; 3:22. [PubMed: 19228404]
128. Wu F, Jeneson JAL, Beard DA. Oxidative ATP synthesis in skeletal muscle is controlled by substrate feedback. Am J Physiol Cell Physiol. 2007a; 292:C115–C124. [PubMed: 16837647]
129. Wu F, Yang F, Vinnakota KC, Beard DA. Computer modeling of mitochondrial tricarboxylic acid cycle, oxidative phosphorylation, metabolite transport, and electrophysiology. J Biol Chem. 2007b; 282(34):24525–24537. [PubMed: 17591785]
130. Wu F, Zhang J, Beard DA. Experimentally observed phenomena on cardiac energetics in heart failure emerge from simulations of cardiac metabolism. Proc Natl Acad Sci USA. 2009b; 106(17):7143–7148. [PubMed: 19357309]
131. Wu F, Zhang EY, Zhang J, Bache RJ, Beard DA. Phosphate metabolite concentrations and ATP hydrolysis potential in normal and ischaemic hearts. J Physiol. 2008; 586(17):4193–208. [PubMed: 18617566]
132. Yipintsoi T, Bassingthwaighte JB. Circulatory transport of iodoantipyrine and water in the isolated dog heart. Circ Res. 1970; 27:461–477. [PubMed: 5452741]
133. Yipintsoi, T.; Bassingthwaighte, JB. Anatomic and functional aspects of the coronary vasculature. In: Hilal, SK., editor. Small Vessel Angiography. St. Louis, MO: Mosby, C. V; 1973a. p. 495-500.
134. Yipintsoi T, Dobbs WA Jr, Scanlon PD, Knopp TJ, Bassingthwaighte JB. Regional distribution of diffusible tracers and carbonized microspheres in the left ventricle of isolated dog hearts. Circ Res. 1973b; 33:573–587. [PubMed: 4752857]
135. Yipintsoi T, Li Z, Kroll K, Feigl EO, Bassingthwaighte JB. Redistribution of regional myocardial blood flow in dog hearts during catecholamine and adenosine infusion. Am J Physiol. 2012; 00:000–000. (under review).
136. Zhou L, Cabrera ME, Huang H, Yuan CL, Monika DK, Sharma N, Bian F, Stanley WC. Parallel activation of mitochondrial oxidative metabolism with increased cardiac energy expenditure is not dependent on fatty acid oxidation in pigs. J Physiol. 2007; 579(3):811–821. [PubMed: 17185335]
137. Zhou L, Cabrera ME, Okere IC, Sharma N, Stanley WC. Regulation of myocardial substrate metabolism during increased energy expenditure: insights from computational studies. Am J Physiol Heart Circ Physiol. 2006; 291(3):H1036–H1046. [PubMed: 16603683]
138. Zhou L, Salem JE, Saidel GM, Stanley WC, Cabrera ME. Mechanistic model of cardiac energy metabolism predicts localization of glycolysis to cytosolic subdomain during ischemia. Am J Physiol Heart Circ Physiol. 2005; 288(5):H2400–2411. [PubMed: 15681693]

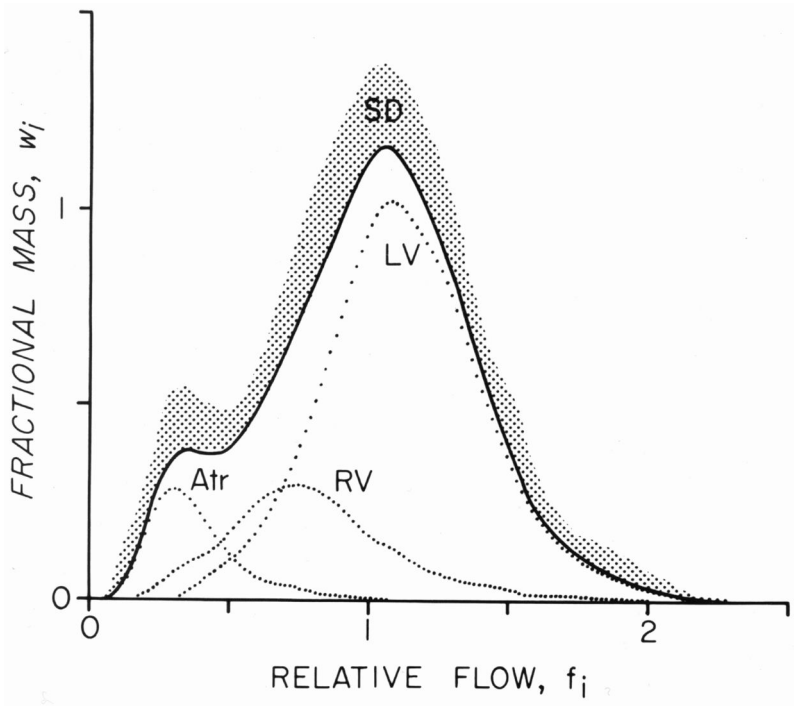

Figure 1.

The probability density function of regional myocardial blood flows relative to the whole heart mean flow from the deposition densities of 15 μm microspheres in the hearts of 13 awake baboons. Data were 4 to 6 estimates in each of 2,706 tissue pieces totalling 13,114 estimates of blood flow per gram of tissue. The solid line is the distribution for the whole heart; the dotted lines are for left ventricle (LV), right ventricle (RV) and atria (Atr). The shaded patch outlines one standard deviation of the f_i in each of the 25 classes of relative flows for the whole heart, where each class width is 10% of the mean flow, and the number of distributions was 67. The area under each curve represents the fraction of heart weight: LV 70%, RV 20% and atria 10%. The mean regional flow relative to the heart mean were LV 1.14, RV 0.81, and atria 0.41. From an average of 208 tissue pieces per heart, the relative dispersion, RD, for the flow heterogeneity, defined as the standard deviation divided by the mean, was: whole heart 0.38, for LV 0.30, RV 0.32, and atria 0.17. (From King et al.[74])

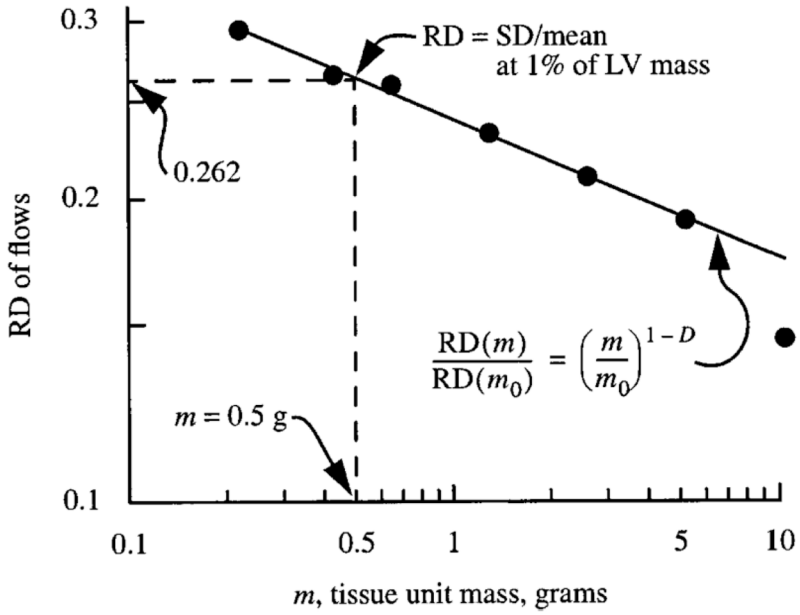

Figure 2.

Normalization of heterogeneity estimate. The RD, relative dispersion of regional flows, is the standard deviation of the regional flows in regions of size m in grams divided by the mean flow for all the regions together, in this case the whole left ventricle, LV. The LV mass was 50 g. The dashed vertical line at 0.5 g, 1% of LV mass, intercepts the observed fractal relationship at RD = 0.262. The regression equation is $RD(m) = 0.232\ (m/m_0)^{-0.18}$ using $m_0 = 1$ g. The fractal dimension $D = 1.18$ or H = 0.82. (Data are from 11 sheep. See Bassingthwaighte King and Roger [16] 1989.)

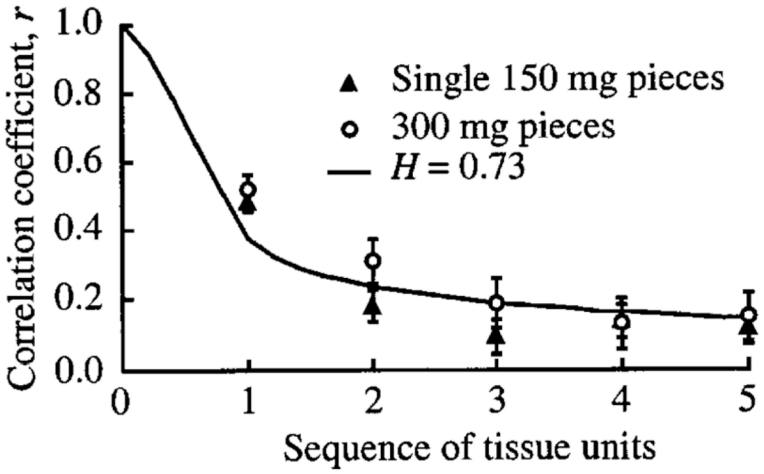

Figure 3.

Correlation between flows in successive tissue units in a series. Sequence number 1 means adjacent units. The correlation, given by the line described by Eq. 1, falls off similarly for 150-mg units (▲) and 300-mg units (○), even though the latter are actually twice the distance between centers. A value of $H = 0.73$ or $D = 1.27$ describes the falloff.

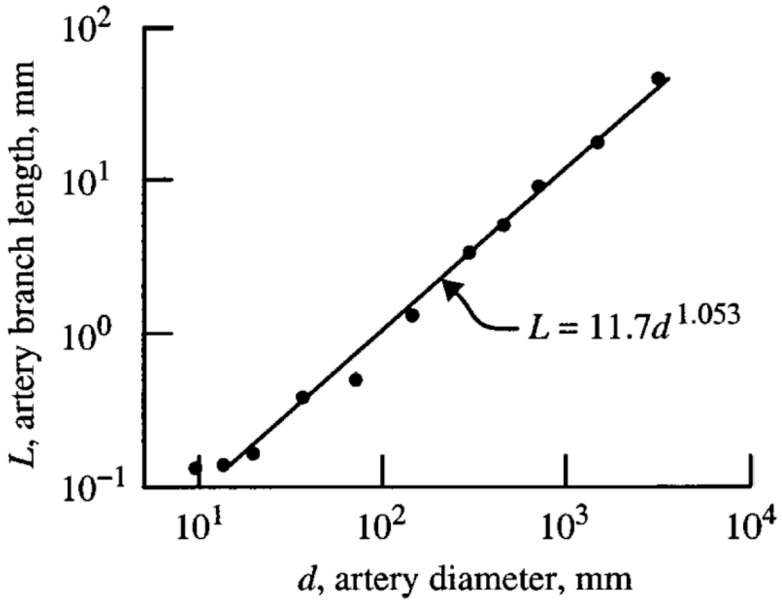

Figure 4.

Analysis of casts of the coronary left anterior descending arterial tree of a pig heart: length, *L*, of average element (i.e., segments in series) of a given generation versus the average diameter, *d*, of the lumen. The logarithmic slope is 1.053. (The data points are average values from Kassab[70], Table 1, left anterior descending coronary artery.)

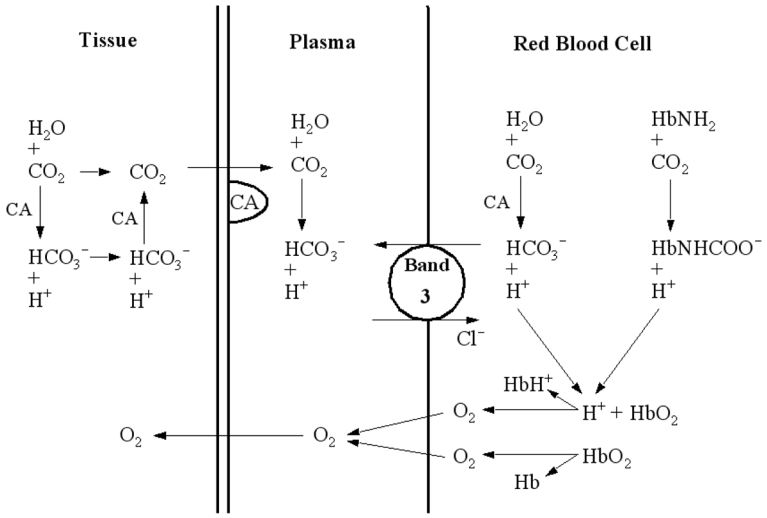

Figure 5.

Schematic diagram of the physiochemical processes that influence the simultaneous blood-tissue exchange of O_2 and CO_2. CA is carbonic anhydrase, the enzyme accelerating the CO_2 hydration reaction inside the RBCs and tissue. The HCO_3^-/Cl^- exchange between plasma and RBCs occurs through the band-3 anion channels on the membrane of RBCs, satisfying the Gibbs-Donnan electrochemical equilibrium principle. [Figure from Geers[54]]

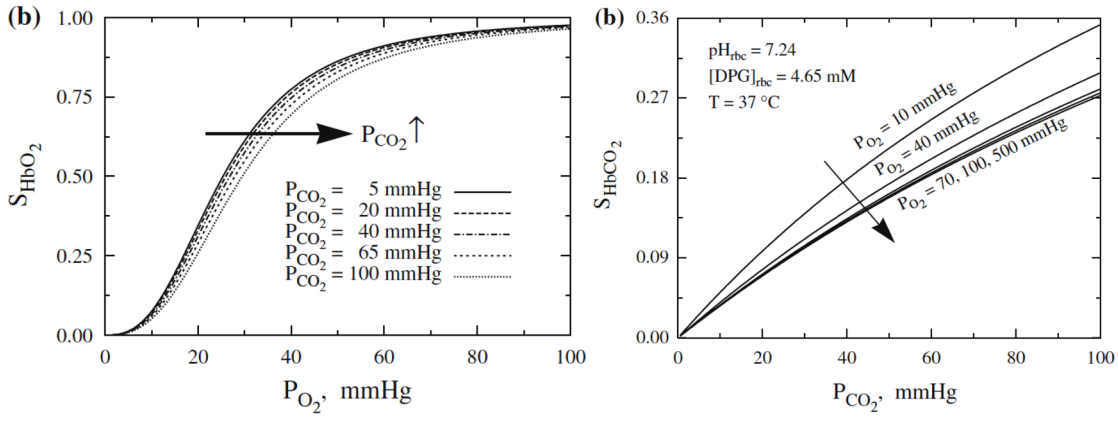

Figure 6.

Bohr and Haldane effects. *Left:* Bohr: Increasing P_{CO2} decreases the affinity of Hb for O_2, shifting the oxy-Hb dissociation curve down and to the right. Right: Haldane: Increasing P_{O2} deceases the affinity of Hb for CO_2 shifting the carboxy-Hb dissociation curve down and to the right. The Bohr effect aids release of O_2 in metabolizing tissues; the Haldane effect aids release of CO_2 in lung capillaries. (Adapted from Dash[45])

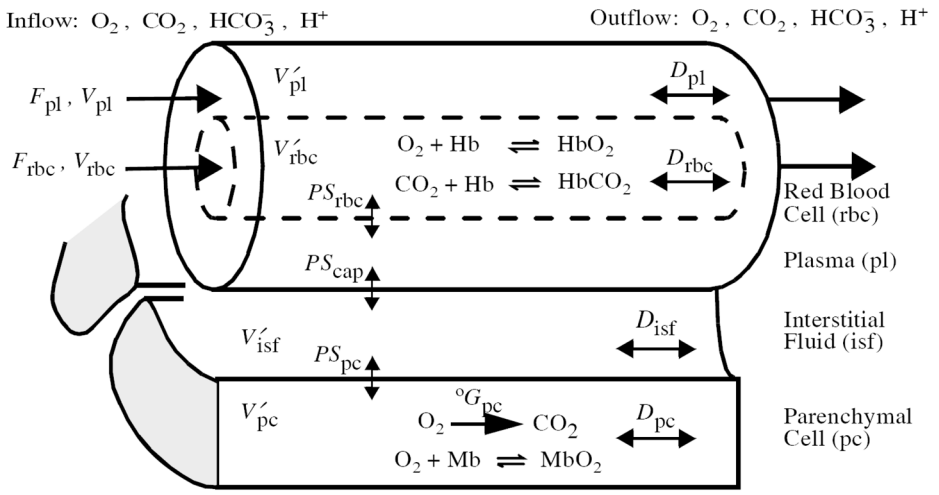

Figure 7.

Schematic diagram of a four-region, axially distributed, blood–tissue exchange (BTEX) model for advection, diffusion, permeation, reaction, and binding of oxygen (O_2), carbon dioxide (CO_2), bicarbonate (HCO_3^-), and hydrogen ions (H^+) in the heart. Endothelial cells region in the capillary membrane were ignored. Detailed kinetics of the binding of O_2 and CO_2 to hemoglobin (Hb) in blood (nonlinear O_2-CO_2 interactions) and the binding of O_2 to myoglobin (Mb) in the parenchymal cells were considered. For the four species, there are four four-region models in parallel. Consumption of O_2 and production of CO_2 occurred only in the parenchymal cells, ignoring O_2 utilization elsewhere. Detailed cellular metabolism leading to consumption of O_2 and production of CO_2 was ignored. The rates of CO_2 production and O_2 consumption were phenomenologically related to respiratory quotient (RQ) which was set 1.0 for glucose metabolism, 0.8 for fat metabolism, and 0.7 for protein metabolism, averaging about 0.8 in normal physiological conditions. F denotes blood flow, V denotes anatomical volumes, V' denotes the effective water spaces (including binding spaces), PS denotes permeability surface area product, D denotes the effective axial diffusion (dispersion), and G denotes the rate of O_2 consumption and CO_2 production; rbc: red blood cells, pl: plasma, isf: interstitial fluid, pc: parenchymal cells. (The figure is taken from Dash and Bassingthwaighte[44] with permission.)

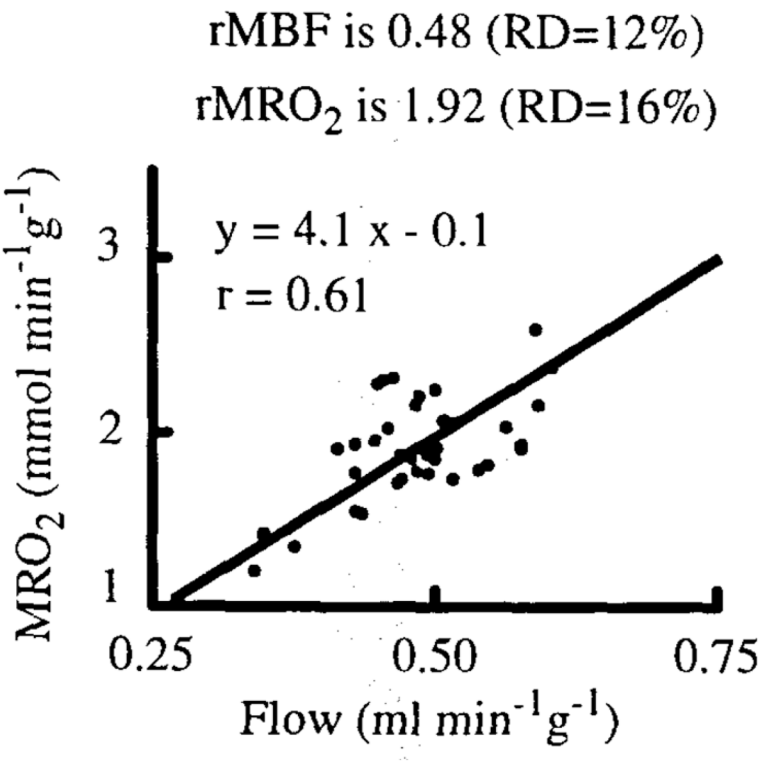

Figure 8.
Correlation between blood flow (rMBF) and oxygen consumption (rMRO2) in regions of interest (size 0.9 ± 0.3 g) of the LV myocardium of a closed-chest dog. (From Li et al.[82])

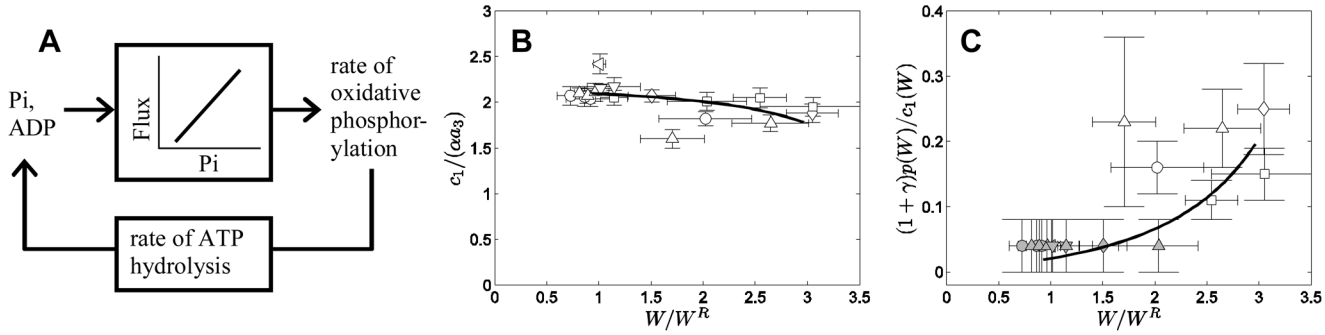

Figure 9.

Feedback control of oxidative phosphorylation in the heart. Diagram in panel A illustrates feedback-mediated control of oxidative phosphorylation in the heart. Panels B and C illustrate the simple two parameter model P_i- and ADP-driven control developed in Beard[27]. The two adjustable parameters in the model are the apparent Michaelis-Menten constants for the ADP and the Pi stimulation of ATP synthesis; they were measured *in vitro* and not adjusted but, as shown, fit the data well within the experimental variance. Data in B and C are adapted from Atkinson[6], Chance[40];Jeneson[69]; Vicini[123]; Balaban[7] ; Wu[128]. Figure reprinted from Beard[27] with permission.

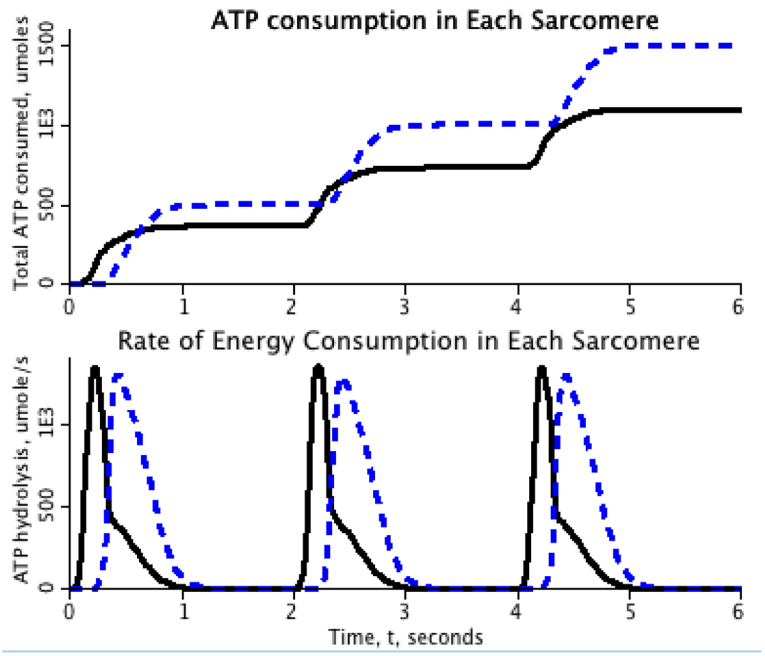

Figure 10.

Energy use in two muscle segments in series. *Black:* Early activated contraction. *Dashed blue:* Late activated and prestretched segment, with the result that contraction is stronger and more energy used. (From Carlson in Bassingthwaighte[10])

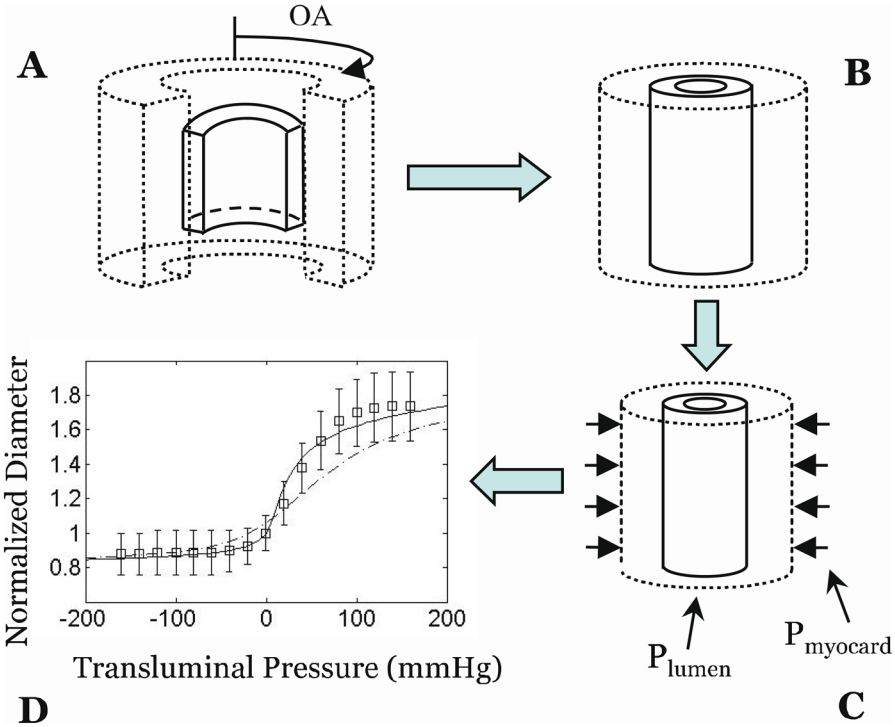

Figure 11.

Myocardium-vessel interaction analysis of diameter, D vs. transluminal pressure, ΔP. A: Myocardium and vessel are stress-free with opening angle OA. B: The closed, unloaded (not stress-free) configuration. C: The system is loaded by external (myocardium induced, $P_{myocard}$) and internal (blood pressure induced, P_{lumen}) pressures. D: The predicted D(ΔP) relationship (solid line) compared to data (rectangles). (Adapted from Algranati[4] with permission).